Magnetic Quartz Crystal Microbalance

A Thesis
Presented to
The Academic Faculty

by

George Y. Yu

In Partial Fulfillment
of the Requirements for the Degree
Doctor of Philosophy

School of Electrical and Computer Engineering
Georgia Institute of Technology
Aug. 2008

Magnetic Quartz Crystal Microbalance

Approved by:

Dr. Jiří Janata, Chair
School of Chemistry and Biochemistry
Georgia Institute of Technology

Dr. Mark G. Allen
School of Electrical and Computer Engineering
Georgia Institute of Technology

Dr. Oliver Brand
School of Electrical and Computer Engineering
Georgia Institute of Technology

Dr. Ian T. Ferguson
School of Electrical and Computer Engineering
Georgia Institute of Technology

Dr. William D. Hunt
School of Electrical and Computer Engineering
Georgia Institute of Technology

Dr. Andrew Lyon
School of Chemistry and Biochemistry
Georgia Institute of Technology

Date Approved: June 11, 2008

This dissertation is dedicated to my family.

Jun Yang and Dong Fang Yu:

thank you for your love, encouragement, and support.

ACKNOWLEDGEMENTS

Through the rewarding journey of graduate school, there were guides and companions. The first and most important guide is my advisor, Prof. Jiří(Art) Janata. From the young graduate student, he led me though many challenges and transformed me. He was always there to welcome my successes and problems alike, never failing to give me encouragement and suggestions.

The path on this journey is well tread with the footsteps of many predecessors. Prof. Wiiliam Hunt, Prof. Ian Ferguson, Prof. Andrew Lyon, Prof. Mark Allen, and Prof. Oliver Brand on my thesis committee have walked this path before. Their experience, support, and encouragement have truly made a difference on my journey.

Certainly, this journey was not made alone. Mira Josowicz who was like a mother to me guided through many difficulties with her expertise and words of encouragement. Through my struggles and successes my fellow group members shared my disappointments and joy. Here, I would like to extend my gratitude to Anthony Smith, Isao Sasaki, Hang Chen, Ryan Cantor, Greg Moakes, Amir Saheb, Jennifer Steeb, and Alex Jonke. Extra special thanks must be given to Anthony Smith, who introduced me to Dr. Janata, Isao Sasaki, Ryan Cantor, and Greg Moakes for their friendship.

Friends have always been important to me. During my journey there was no shortage of great friendships. Some started as office-mates, others through adventures and friends. I would like to give thanks to my friends; Anthony Smith, Isao Sasaki, Ryan Cantor, Greg Moakes, Anne Mclaughlin, Tom Drews, Anna Adams, and Mina Sartipi. They have added laughter, happiness, and comfort to my journey. I would like to give extra special thanks to my girlfriend Mina. In the last three years of my journey, when the journey gets hard Mina was always there to encourage me, push me, support me, and love me. Mina, thank you.

To many, paper works are done automatically, the garbage seems to disappear every

night, and the floors magically stay clean. Certainly, that is not true. Everyday I come to work, I appreciate the hard work of the staff for making my work possible.

One must remember those who made this journey possible. The years of changing diapers, enduring cry for milk, stubborn outbursts, and requests for more money coupled with many hugs, kisses, and love have made this journey possible. My greatest thanks and love to my parents, Jun and Dong-Fang. Although, they were miles and miles away from me, but their love and support were always with me.

TABLE OF CONTENTS

LIST OF TABLES

LIST OF FIGURES

SUMMARY

In this thesis, a new technique for using quartz crystal microbalance (QCM) in magnetic field was explored. This technique would take advantage of the sensitive nature of QCM to vibration changes. The idea is to perturb the QCM vibrations with magnetic materials on it by applying magnetic field. A new instrument called magnetic QCM (MQCM) was constructed to explore this technique.

The thesis is divided into three bodies of work. The first body describes the development of the MQCM instrument and the demonstration of the technique. The resonance frequency of a QCM with conducting polymer (polyaniline) suspension in poly(ethylene glycol) was observed to increase with increasing the externally applied uniform DC magnetic field. Slowly sweeping the magnetic field between 0 and 3.1 T results in a frequency-field response curve. Chemical doping was done by exposing the polyaniline-emeraldine base film to HCl vapor. The change in population of free spins is reflected in increased frequency-field curve magnitude after HCl doping. Two working hypothesis explaining this observation are offered to explain how frequency of QCM with deposited magnetic film shifts with increasing intensity of the magnetic field.

The second body of work describes the study of QCM proximity phenomenon discovered during the development process of the MQCM instrument. When an object approaches a vibrating quartz crystal microbalance (QCM) the resonant frequency changes. This "proximity effect" is seen at the distance of 10 mm in air and becomes more pronounced as the distance decreases. This effect depends on the value of quality factor (Q-factor), conductivity of the object, and electrical connection of the object to the QCM electrodes. The proximity effect is largest (>200 Hz for 10 MHz QCM) when the Q-factor is low (< 1000) and a conducting metal plate (e.g. Cu) is electrically shorted to the proximal (nearest) QCM electrode. The finite element modeling shows that the effect is likely due to capacitive interaction of the object with the fringing electromagnetic field of the QCM. A simple

modified Butterworth Van-dyke model is used to describe this effect. It must be recognized that this effect may lead to large experimental artifacts in a variety of analytical QCM applications where Q-factor changes. Therefore, in order to avoid artifacts, QCMs and similar mass acoustic devices should not operate in low Q-factor (< 1000) regime.

The third body of work describes an improved 2nd version of MQCM and in this work the complex geometry such as particle suspension were simplified to alternating stack of ferromagnetic and diamagnetic layers. When external magnetic fields of up to 10kG was applied, changes in the QCM admittance magnitude and phase curves were observed. A mass-equivalent stack of continuous consecutive layers of nickel and gold was also exposed to magnetic field but no admittance magnitude and phase changes were observed. Butterworth-van-Dyke (BVD) model was used to mimic the observed effects by varying only the equivalent resistor component. Since the resistor component changes in BVD model are attributed to internal shear friction effects among other losses, it indicates that the friction at the nickel/gold interface is modulated by the magnetic field. Quantum effect similar to giant magnetoresistance (GMR) was considered. However, after examining SEM surface images, the sources of acoustic response to magnetic field is more likely coming from material interfacial stresses and not from the quantum effects.

Overall, this thesis has opened a new research area that combines the sensitive nature of piezoelectric resonators such as the QCM and magnetic materials. The results from experiments point to the importance of interfacial stress in the transduction principle of MQCM.

CHAPTER I

INTRODUCTION

This chapter explains the background on quartz crystal microbalance (QCM), magnetism, motivation for developing the magnetic QCM (MQCM), and the brief descriptions of experiments performed with the MQCM instrument.

1.1 *Quartz Crystal Microbalance*

1.1.1 General

The piezoelectric effect or piezoelectricity is the ability of certain crystals to generate an electric field from an externally applied mechanical stress. The effect is reversible, in which the electric field can slightly change the shape of a crystal by producing stress and/or strain. Crystals such as quartz can be cut at certain angles (Figure 1) to produce certain geometries with select resonance frequencies of very high quality factor (ratio of frequency and bandwidth defined in Eq. 1). Because of the extremely high quality factor resonance frequencies, piezoelectric crystals were first utilized in electronic filters by W. G. Cady [7]. Applications for such piezoelectric crystal have later developed into areas such as high-voltage sources, actuators, frequency control, and ultrasonic transducers. However, it was Sauerbrey who used a quartz crystal to determine very small mass ($\Delta f = 0.233 Hz/ng/cm^2$ for 10 MHz AT-cut QCM calculated from [17])changes in a thin film [46], and the device became known as the quartz crystal microbalance (QCM). They are often used in the semiconductor industry for measuring and controlling the thickness of film depositions and used as mass sensors $[1, 16, 24, 28, 31, 32, 50]$.

$$Q\text{-Factor} = \frac{f_0}{\Delta f} \ ,$$

$$\Delta f = \text{Half power resonant bandwidth}$$

$$f_0 = \text{Resonant frequency}$$

(1)

1.1.2 Working Principle

QCM is a transducer consisting of two metal electrodes evaporated on opposite sides of a thin piezoelectric quartz plate. The geometry and boundary conditions allow a resonating acoustic transverse shear wave in the quartz plate (Figure 2). The thickness (d) and acoustic shear wave velocity (V) of the quartz determines the fundamental resonance frequency in Eq. 2 where λ is the wavelength.

$$
\begin{aligned}
f_0 &= V/d \ , \\
d &= \lambda/2
\end{aligned}
\tag{2}
$$

1.1.3 Modes of Operation

QCM is usually operated in conjunction with an economical oscillator circuit [2]. In this mode, a oscillator circuit excites a QCM and feeds back an amplified response from the QCM. Because of the feedback loop, the circuit will oscillate at the resonating frequency. A circuit cutoff switch can be added to the oscillator circuit to switch off the excitation voltage and measure the decaying sine wave of the QCM voltage [45, 48]. The decay rate parameters add another dimension to the oscillator mode of operation.
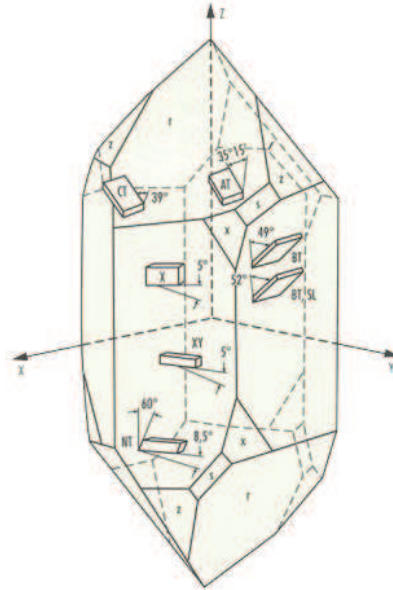
Figure 1: Different resonator cuts of a quartz crystal.

QCM can also be driven by network analysis of impedance or admittance in which a frequency sweeping excitation sine wave is applied to a QCM. The electric conductance as a function of excitation frequency can determined by a network analyzer.

1.1.4 Effects of Temperature and Stress

The resonance frequency of a QCM is dependent on temperature, stress, and pressure. Different cuts of quartz (Figure 1) reacts differently to these parameters. The temperature dependance of different cut QCM is shown in Figure 3. In this graph, the widely popular AT-cut QCM show the greatest temperature stability at room temperature compared with other cuts of quartz crystal.

1.1.5 Small-Load Approximation

Acoustic resonators are often modeled with equivalent electrical circuits. Equivalent circuits are the electrical equivalent to the mechanical and acoustic reflectivity descriptions [42]. The impedance analysis of a QCM can be modeled using the Butterworth-van-Dyke (BVD) model shown in Figure 4. The BVD model is composed of a motional arm described by the circuit components; resistor (R_1), capacitor (C_1), and inductor (L_1), and electrical arm described by the capacitor (C_0) component. The C_1 capacitor represents the mechanical
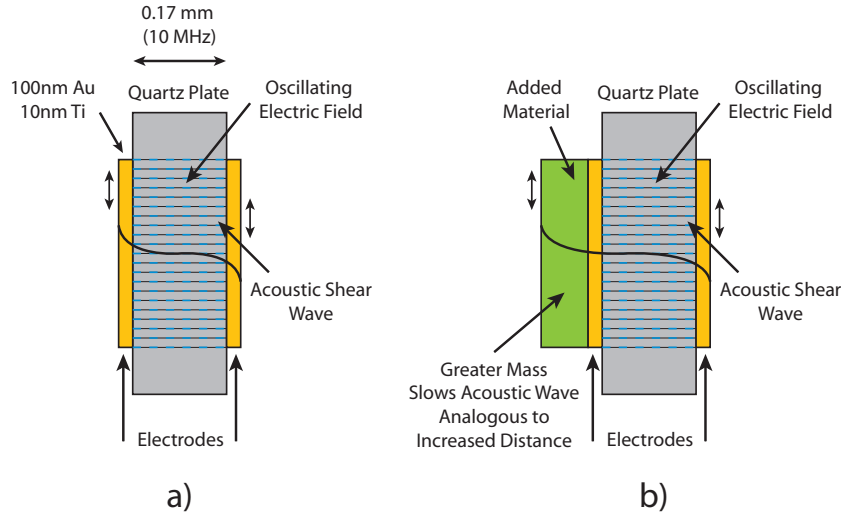
Figure 2: a) Blank QCM oscillating in air with shear waves. b) Materials added to an QCM electrode to alter inertial motion of shear wave translating to a change in resonance frequency.

elasticity of the quartz. The L_1 inductor represents inertial mass. The R_1 resistor represents the energy losses from viscous effects, internal friction, and damping induced by crystal holder. The C_0 capacitor determines the admittance away from resonance, while the motional arm consisting of R_1, L_1 and C_1, dominates the admittance near the resonance [24]. The Z_L component represents the impedance from the load. This value can only be determined by comparing the unloaded and loaded states of a QCM. Assuming a frequency shift is much smaller than the resonant frequency, the frequency shift due to Z_L can be predicted by small-load approximation shown in Eq. 3, where f_0 is the fundamental frequency and Z_{qcm} is the acoustic impedance of the material ($8.8 \cdot 10^6 kg \cdot m^2 \cdot s^{-1}$ for AT-cut quartz).

$$\frac{\Delta f}{f_0} = \frac{j}{\pi Z_{qcm}} Z_L \tag{3}$$

The simplicity of small-load approximation makes the interpretation of QCM data easy and made QCMs widely popular. Since the small-load approximation is the first order
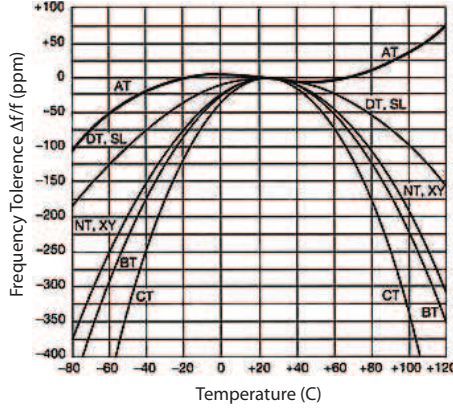
Figure 3: Resonator temperature dependance of different cuts of quartz.
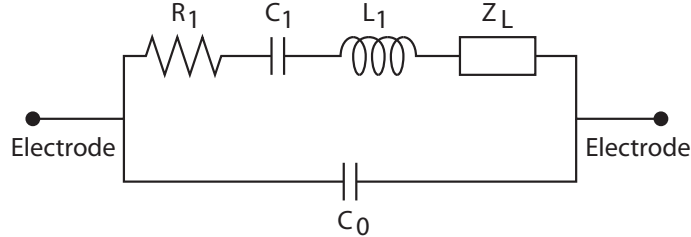
Figure 4: Butterworth-van-Dyke (BVD) model of a QCM.

4

solution of a perturbation analysis [26], the stress to speed relationship is assumed to be linear. If the average stress-to-speed ratio of a sample at the surface can be calculated then the small-load approximation can be used for quantitative analysis. Otherwise, the interpretation has to remain qualitative.

When, the stress to speed relationship is not linear due to surface roughness, phenomena like slip and yield sets in. For these cases, a more generalized small-load approximation equation Eq. 4 can be applied, where, μ_0 is oscillation amplitude and stress $(\sigma(t))$, is periodic in time and synchronous with the crystal oscillation, and ω is the angular frequency.

$$\frac{\Delta f}{f} = \frac{1}{\pi Z_{qcm}} \frac{2}{\omega \mu_0} \sigma(t) cos(\omega t) \tag{4}$$

1.1.6 Inertial Loading

In the classical application of QCM defined by the Sauerbrey equation (Eq. 5), a thin film is assumed to rigidly couple to the crystal. In this case, the stress is governed by inertia, $\sigma = -\omega^2 \mu_0 M_f$, where μ_0 is the amplitude of oscillation and M_f is the average mass per unit area. After inserting the inertia term into the small-load approximation Eq. 4, one arrives at the Sauerbrey equation (Eq. 5), where C_q is a modified version of Z_{qcm} constant.

$$\Delta f = -C_q f_0{}^2 \Delta M_f \tag{5}$$

1.1.7 Electrochemical QCM

Because of the conducting electrodes on a QCM, one of these electrodes can be easily combined with electrochemistry. Such combination is then called Electrochemical QCM (EQCM) [5, 6]. The frequency shift information can be correlated with the amount of charge passed during an electrochemical reaction thereby determining current efficiency.

1.2 Magnetism

All materials are influenced by the presence of a magnetic field. The source of this effect goes all the way to the atomic level (Figure 5). Maxwell's equations have described the relationship between moving charge and magnetic field [34]. The spinning of electrons in their

orbit around the atomic nucleus produces a magnetic moment [38]. Many atoms/molecules have electron spins in opposite directions. By having opposite spins, the magnetic moments will cancel out.

For magnetic materials, a key measure of the magnetic property is the magnetic susceptibility (χ_m), which relates magnetic field (H) and magnetization density (M) in (6). Similar to Equation (6) and (7) are used to describe the relationship between magnetic field flux density (B) and magnetic field (H). The relative magnetic permeability (μ_r) is $1 + \chi_m$. Both (μ_r) and (χ_m) describe the density of magnetic moments that are aligned when a certain magnetic field (H) is applied.

$$M = \chi_m H \tag{6}$$

When there is no or very little net magnetic moment, the material is considered diamagnetic. This is defined as having negative χ_m. In practical terms, diamagnetic materials have such small magnetic moments that room temperature thermal kinetic energy randomly orients the small net magnetic moments in the bulk (Figure 6). If a magnetic field is externally applied to diamagnetic materials, the magnetic moments will not be significantly affected and will remain randomly oriented.
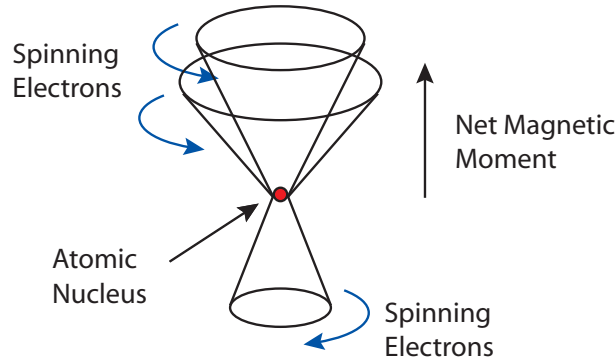
Figure 5: Magnetic dipole from unpaired spinning electrons.

$$B = \mu_r \mu_0 H = \mu_0 (H + M)$$

$$\mu_r = \text{relative permeability} \tag{7}$$

$$\mu_0 = \text{magnetic permeability of vaccum}$$

No External Magnetic Field   Applied External Magnetic Field   No External Magnetic Field
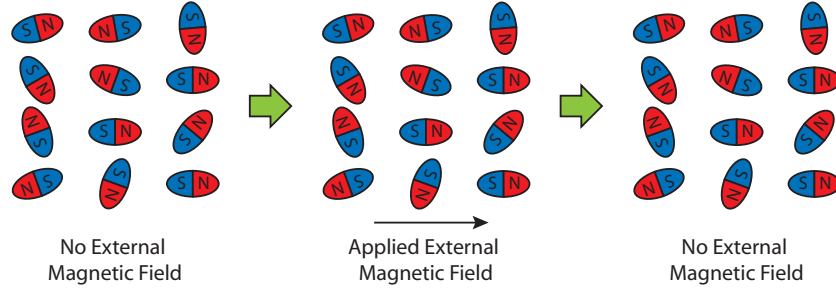
Figure 6: Diamagnetic dipole orientations

Paramagnetic materials have magnetic susceptibility greater than zero and have some net magnetic moments. Paramagnetic materials normally have random orientation of magnetic moments (Figure 7). However, under an externally applied magnetic field, paramagnetic materials will magnetize by orienting their magnetic moments in the direction of the external field. When the external field is removed, a paramagnetic material will return to its normally random oriented magnetic moments.

No External Magnetic Field   Applied External Magnetic Field   No External Magnetic Field
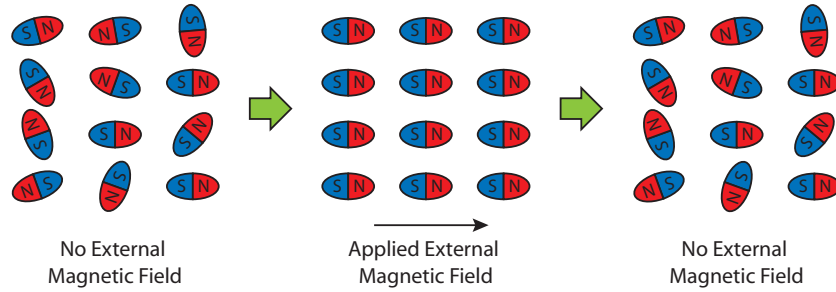
Figure 7: Paramagnetic dipole orientations

Some materials have large net magnetic moments and can be easily magnetized. These material are known as ferromagnetic materials and usually have magnetic susceptibility much greater than zero. Some ferromagnetic materials are normally magnetized at room temperature. However, with enough kinetic energy this magnetization can be randomized (Figure 8). When cooled to room temperature, the dipoles will stay randomized. An

externally applied field can permanently re-magnetize ferromagnetic materials.
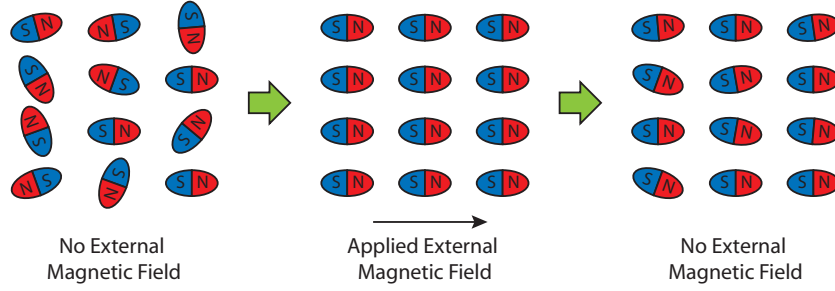
Figure 8: Ferromagnetic dipole orientations

For diamagnetic and paramagnetic materials, the μ_r value is constant, resulting in a linear relationship between B and H. For ferromagnetic materials, μ_r is not constant since the material can be easily saturated at low magnetic fields. The linear $B - H$ relationship only holds for very low field and then a non-linear saturation occurs. The $B - H$ curve is one of the important relationships used to determine μ_r or χ_m.

1.3 Existing Techniques for Measuring Magnetic Properties

Many techniques can measure the $B - H$ curve of materials. Instruments such as Faraday balance, alternating gradient force magnetometer (AGFM or AGM), vibrating sample magnetometer (VSM), and super-conducting quantum interference devices (SQUID) have been around for decades [14].

The Faraday balance technique is the oldest of all the techniques. It works by subjecting a sample material to a gradient magnetic field and measuring the force induced on the sample material (Figure 9). The force can be measured by a variety of weighing methods. This force corresponds to the degree of magnetization. Using an electromagnet, a field gradient sweep and measuring magnetization in the form of induced force on the sample will generate a classic $B - H$ curve.

The alternating gradient force technique shown in Figure 10 uses a superimposed AC gradient field on a DC field to create vibrations in the sample. These vibrations are detected

by a piezoelectric transducer and converted to a voltage signal. Because of the noise, a lock-in amplifier is usually used to amplify the signal at the frequency of the superimposed AC signal. The amplified signal amplitude corresponds to the magnetization of the material at that magnetic field intensity, resulting in a B-H curve.

The vibrating sample technique shown in Figure 11 is one of the more popular techniques for measuring magnetic properties. A sample is vibrated in the Z direction with small amplitude and known frequency in a DC uniform magnetic field. The motion of the sample in the uniform field causes a disturbance to the uniform field in the same frequency as
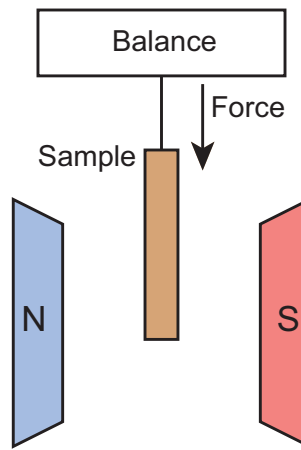
Figure 9: Principle of Faraday balance technique
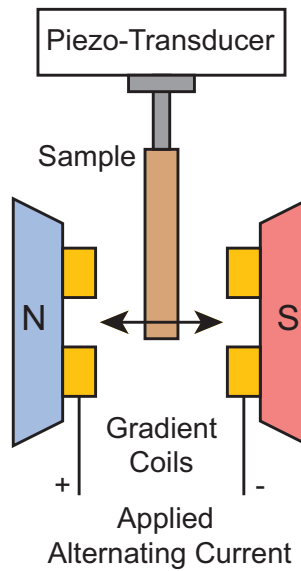
Figure 10: Principle of alternating gradient field technique

the sample vibration. This disturbance can be converted to electrical voltage by a set of induction (pickup) coils. A lock-in amplifier can amplify the signal and measure the signal amplitude. The signal amplitude corresponds to the magnetization of the material at that magnetic field intensity.
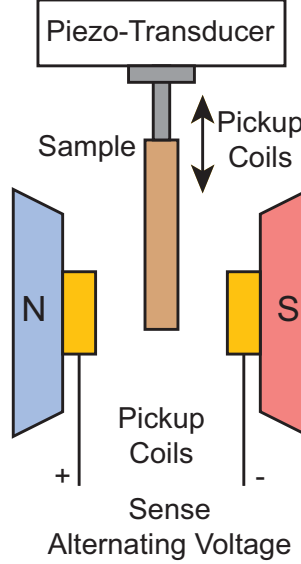
Figure 11: Principle of vibrating sample magnetometer technique

The super-conducting quantum interference technique is the most sensitive technique for measuring magnetic property. This technique, shown in Figure 12, uses two Josephson junctions that have slightly different insulation thickness for the two paths on a superconductor. The Josephson junction will develop a biasing current corresponding to the difference in wave function of the tunneling Cooper pairs. If a constant biasing current is maintained in the SQUID device, the measured voltage oscillates with the phase difference at the two junctions. Since the phase difference at the two junctions depends on the change in the magnetic flux, counting the phase shift in the voltage oscillations allows the measurement of the small magnetization change that has occurred [10].

For all the techniques of magnetic property measuring, very few major advancements have occurred in the last two decades. Recent advancements have just allowed techniques such as VSM and SQUID to measure magnetic properties of thin films, but the film mass must be separately determined. These techniques are well established, but all are based

on the assumption that the magnetic properties of the sample do not change during the measurement. No one has investigated the transient change in material magnetic property during (in-situ) chemical reactions. None of the established techniques can conveniently measure sample properties during a chemical experiment.

1.4 Conducting Polymers and Magnetism

The study of magnetic properties provides important information about new materials. One such group of materials is conducting polymers. In this research, polyaniline (PANI) was used. PANI is a promising material in such areas as organic electronics, gas sensors, and batteries [51].

Polyaniline was first known in 1835 as "aniline black." There are five oxidation states of polyaniline: leucoemeraldine, protoemeraldine, emeraldine, nigraniline, and pernigraniline. Leucoemeraldine is the most reduced form of polyaniline and Pernigraniline is the most oxidized form of polyaniline [51]. Of the five oxidation states, each one can exist in the base or the protonated (salt) form (Figure 13). Neither reduced nor oxidized extremes of polyaniline is interesting because they either do not have enough carriers or too much paired carriers to conduct. Therefore, the most interesting form of polyaniline is the emeraldine form.
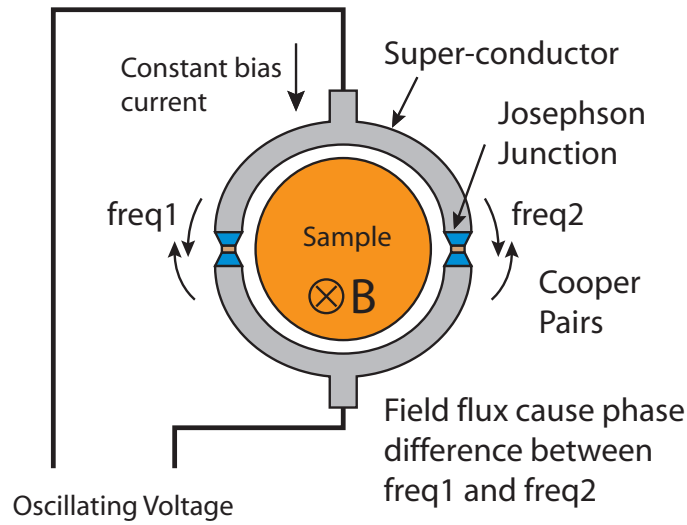
Figure 12: Principle of superconducting interference technique

In the base form of polyaniline emeraldine, the material is not very conductive because of very few carriers. However, when it is doped or protonated it becomes conductive because of the hole carriers are formed from protonation. This property of polyaniline makes it similar to a p-type semiconductor. PANI conductivity can then be modulated by gas or voltage to either enhance or quench the free carriers. This property of PANI makes it attractive for use in chemical sensors or as an organic material for organic electronics. The conductivity of a material is also often tied to magnetic property because of the existence of unpaired electron spins. Some studies have been done to investigate the magnetic properties of PANI [30, 37, 39]. However, a great deal is still unknown about the magnetic properties of this material.
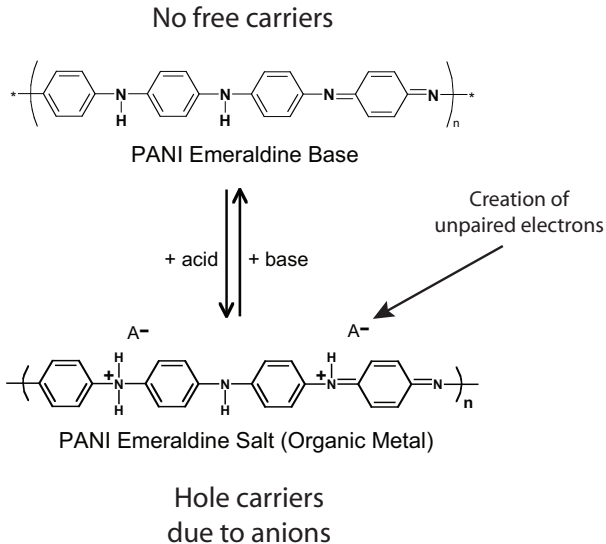
Figure 13: Base and salt form of Polyaniline.

1.5 The Problem and Motivation for New Technique

Past research [23] has already established that specially modified PANI changes its conductivity and work function when exposed to certain gases. PANI is an organic semiconductor and can be modified to create a chemically selective sensor for various gases [22]. It has been surmised that similar to changes in electrical properties when exposed to gases, the magnetic properties of PANI would also be affected. The magnetic properties may provide additional insight into gas/solid interactions of PANI, spintronics, and other applications of organic

semiconductors. Thus, in-situ magnetic property measurement is potentially important for conducting polymers because many of the effects of gases on these materials are both reversible and irreversible. The lack of in-situ measurement capability of other techniques motivated the creation of a new style of instrument for in-situ characterization of material magnetic properties. The first inspiration came from the work of Grebennikov et al. [18], who reported on operation of quartz crystal microbalance (QCM) in a non-homogeneous magnetic field generated by a permanent magnet with shaped poles. Our attempt to replicate their non-homogeneous, static magnetic field experiment yielded a similar result in a homogeneous field. However, we extended our approach to operation of the QCM in a scanned homogeneous magnetic field.

1.6 Development of MQCM

A new technique for measurement of magnetic properties of materials is demonstrated. It can be used for the measurement of thin magnetic films during their chemical modification. The resonance frequency of a QCM with conducting polymer (polyaniline) suspension in poly(ethylene glycol) was observed to increase with increasing the externally applied uniform DC magnetic field. Slowly sweeping the magnetic field between 0 and 3.1 T results in a frequency-field response curve. Chemical doping was done by exposing the polyaniline-emeraldine base film to HCl vapor. The change in population of free spins is reflected in increased frequency-field curve magnitude after HCl doping. Two working hypothesis explaining this observation are offered to explain how frequency of QCM with deposited magnetic film shifts with increasing intensity of the magnetic field.

1.7 Proximity Effect in QCM

During the development process of the MQCM instrument, the QCM proximity phenomenon was discovered. When an object approaches a vibrating quartz crystal microbalance (QCM) the resonant frequency changes. This "proximity effect" is seen at the distance of 10 mm in air and becomes more pronounced as the distance decreases. This effect depends on the value of quality factor (Q-factor), conductivity of the object, and electrical connection of the

object to the QCM electrodes. The proximity effect is largest (>200 Hz for 10 MHz QCM) when the Q-factor is low (< 1000) and a conducting metal plate (e.g. Cu) is electrically shorted to the proximal (nearest) QCM electrode. The finite element modeling shows that the effect is likely due to capacitive interaction of the object with the fringing electromagnetic field of the QCM. A simple modified Butterworth Van-dyke model is used to describe this effect. It must be recognized that this effect may lead to large experimental artifacts in a variety of analytical QCM applications where Q-factor changes. Therefore, in order to avoid artifacts, QCMs and similar mass acoustic devices should not operate in low Q-factor (< 1000) regime.

1.8   MQCM Multi-layer Stack

A stack of alternating layers of nickel and gold was electroplated on a quartz crystal microbalance (QCM). When external magnetic fields of up to 10kG was applied, changes in the QCM admittance magnitude and phase curves were observed. A mass-equivalent stack of continuous consecutive layers of nickel and gold was also exposed to magnetic field but no admittance magnitude and phase changes were observed. Butterworth-van-Dyke (BVD) model was used to mimic the observed effects by varying only the equivalent resistor component. Since the resistor component changes in BVD model are attributed to internal shear friction effects among other losses, it indicates that the friction at the nickel/gold interface is modulated by the magnetic field.

CHAPTER II

DEVELOPMENT OF MQCM

In this work, the design of the first MQCM instrument and engineering specifications were described. Using the first MQCM instrument, a set of experiment was done to validate the ability of MQCM to detect different concentrations of the paramagnetic material, polyaniline (PANI). Because of the successful validation of MQCM ability with PANI, a further experiment was done to test ability of MQCM to detect changes to magnetic properties of PANI by doping.

2.1 Magnetic Quartz Crystal Microbalance (MQCM) Concept

QCMs can be an extremely sensitive detection tool for physical changes of material properties, such as elasticity, surface viscosity, interfacial properties of multi-layers, etc. [24]. It has been surmised that magnetic materials deposited on an oscillating QCM and subjected to strong non-homogeneous magnetic field develop a force perturbation that changes the resonant frequency [18]. The goal in developing our instrument is to use a QCM to measure in-situ magnetic properties of thin films of conducting polymers, namely, during their exposure to various chemicals and chemical reactions. This new style of instrument provides the combination of mass and magnetic measurements using the same device. This new instrument is called magnetic quartz crystal microbalance (MQCM). The extremely sensitive nature of piezoelectric acoustic perturbation could also promise a greater level of sensitivity with higher frequency devices used for mass measurements, such as for example, surface acoustic wave devices (SAW).

In the past, there were some studies on liquid phase QCM operation and electromagnetic excitation of thickness-shear mode (TSM) piezoelectric sensor in liquid [52,56]. Their results showed an amplitude enhancement effect on TSM sensors by electromagnetic excitation and

pointed to a possibility of QCM being used as a tool for measuring magnetic properties. R. Brendel et al. reported on the effect of magnetic field on piezoelectric resonators [3, 4]. Their studies showed that if magnetic materials are used as supports for the quartz crystal resonators, stresses from these supports induced by the magnetic field will alter the resonance frequency of the resonator.

2.2   DESIGN AND CONSTRUCTION

2.2.1   Overall system description

The MQCM system diagram is shown in Figure 14. The system consists of an electromagnet, field control, field measurement, QCM, oscillator, frequency counter, digital multi-meter, and sample chamber. A photograph of the MQCM system is shown in Figure 15.
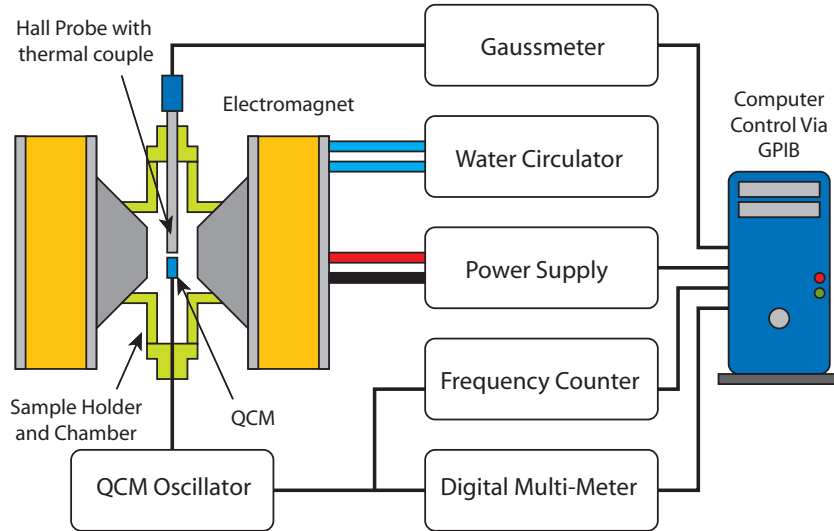
Figure 14: Magnetic Quartz Microbalance (MQCM) system diagram.

2.2.2   Electromagnet

An electromagnet is used to generate the uniform magnetic field. The electromagnet in the current system is a GMW H-frame model 3473-70 capable of 70A current. The 50 mm diameter flat face magnet pole caps with tapered edges are used. The gap between the magnet poles is set to about 6 mm. The ultra flat pole faces provide a highly uniform magnetic field. This and the scanning mode are the major differences between our design

and the previously reported system [18]. The magnet is water cooled with a heat exchanger connected to an external water supply. The magnet coil temperature is kept at around 19 degrees C +/- 1 degree.

2.2.3 Field control and measurement

The electromagnet is powered by a PowerTen R62 60 V, 110 A programmable power supply. This power supply is capable of 0.0269 A current step resolution and stability of 0.05 % over 8 hours. Because the magnet pole material will saturate around 2 T, the magnetic field flux density does not vary linearly with current passing through the magnet coils. The magnet pole spacing will also result in different current vs. magnetic field flux density curves. With this power supply and magnet pole gap configuration, the maximum magnetic field flux density that can be achieved is around 32 kG (3.2 Tesla) in air. The magnet also includes a residual field flux of around 350 to 420 G. The field measurement is made by a Lakeshore HMMT-6J04-VR Hall probe and Lakeshore 455DSP gaussmeter set. This measurement set is capable of measuring magnetic field flux density from 35 G to 35 kG at 5-digit precision. It is also temperature compensated and includes a thermocouple of 0.01 degree C resolution at the Hall probe tip. The field control schemes implemented in the current instrument
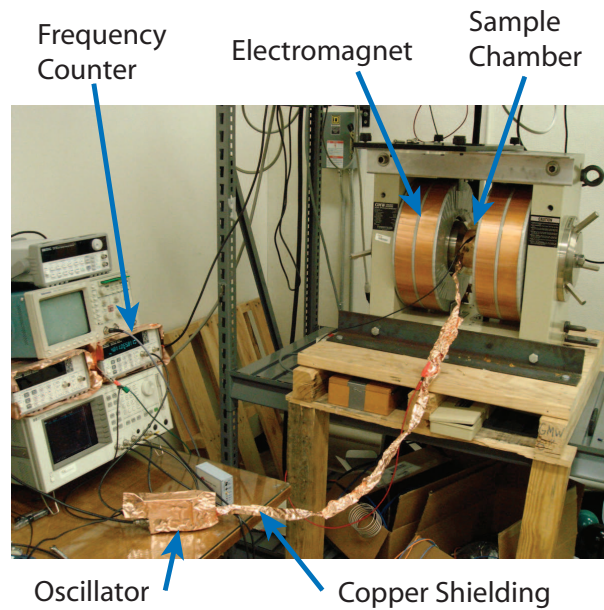
Figure 15: Photograph of MQCM setup.

are either current control only or current control with Hall probe feedback. For ramping the magnetic field intensity (H), a pre-established H vs. current calibration curve is used to directly control current instead of feedback control. For more stability, a Hall probe feedback control of current is used with the help of a computer.

2.2.4   QCM crystal and oscillator

The system used 10 MHz AT-cut etched QCMs of 13.67 mm diameter with 5.1 mm diameter electrodes (International Crystal Manufacture Inc.). The electrode material consists of a 10 nm Ti adhesion layer and a 100 nm Au layer. The QCM is operated by a Maxtek PLO-10i phase lock oscillator (5.1 to 10MHz). The oscillator outputs the QCM frequency and the admittance as an amplified analog voltage.

2.2.5   Frequency counter and digital multi-meter

The QCM resonance frequency information from the oscillator is acquired by an HP 53131A frequency counter. The frequency counter is then interfaced with the computer via a general purpose interface bus (GPIB) serial cable. The QCM admittance information is acquired by an HP 34401A digital multi-meter. A computer is used to provide complex control sequences and multiple data acquisition. The program LabView is used in conjunction with a GPIB PCI board to communicate with the instruments.

2.2.6   Sample holder and measurement chamber

The custom engineered sample chamber consists of five identical ports (Figure 16). The sample holder is used to provide mechanical support for the QCM as well as electrical connection to the two QCM electrodes. It was designed to fit into one of the five ports. The mechanical support is provided by two gold plated clips soldered (60/40 tin/lead) to two copper tubes. The copper tubes leads extending outside of the high magnetic field area were connected to solid wires via solder. The wires were then connected to a BNC connector. The sample holder, sample chamber, and other accessories were made from Vantico 5510 resin using a rapid prototyping stereolithography technique. The copper tube electrical leads, brass gas tubes, and Hall probe were sealed using Loctite 404 glue. O-rings seal each

port by compression. The sample chamber is sealed to the magnet poles by two large Viton O-rings.

2.2.7 Wiring and shielding

It was found that wiring and electronic shielding precautions must be taken to eliminate interference from the strong magnetic field or the magnet power supply The small inductance on any twisted braided wires is affected by even a slow sweep of the applied field. Therefore, solid core wires must be used to connect the QCM to the oscillator. The magnet power supply also produces a great deal of electromagnetic interference affecting the QCM oscillator loop. This loop must be shielded to establish an interference-free cavity. The shielding as well as one of the QCM electrodes must be connected to the power supply ground.

The sample chamber is designed to provide a gas-tight seal for nitrogen or a low-vacuum environment. However, because of residual electronic interferences, the sample chamber must be lined by a layer of copper foil, which makes the realization of gas tight seal difficult.

2.3 EXPERIMENTAL PROTOCOL

2.3.1 Film preparation

A set of preliminary experiments was performed to demonstrate the feasibility of the MQCM system. PANI emeraldine base (PANI-EB) powder of 5,000 molecular weight (mw), as the sample material was suspended in poly(ethylene glycol) (PEG) of 4,000 mw. A solution of 7.5 %wt of PEG in water was prepared for mixing with PANI-EB powder in ratios of 0 mg, 4 mg, 8 mg, and 16 mg PANI-EB to 4 ml of PEG solution. The resulting PANI to PEG concentrations are 0 %wt, 1.3 %wt, 2.7 %wt, and 5.3 %wt, respectively. The mixtures were then shaken until the PANI powder was dispersed in the solution. Four QCMs were selected for deposition of the composite via spin casting. After each crystal was flooded by a particular solution mixture, it was spun at 600 rpm for 15 minutes and then dried at room temperature. The spin-casting and drying processes were repeated three times, yielding a composite film with suspended PANI particles. A micrograph of this type of film
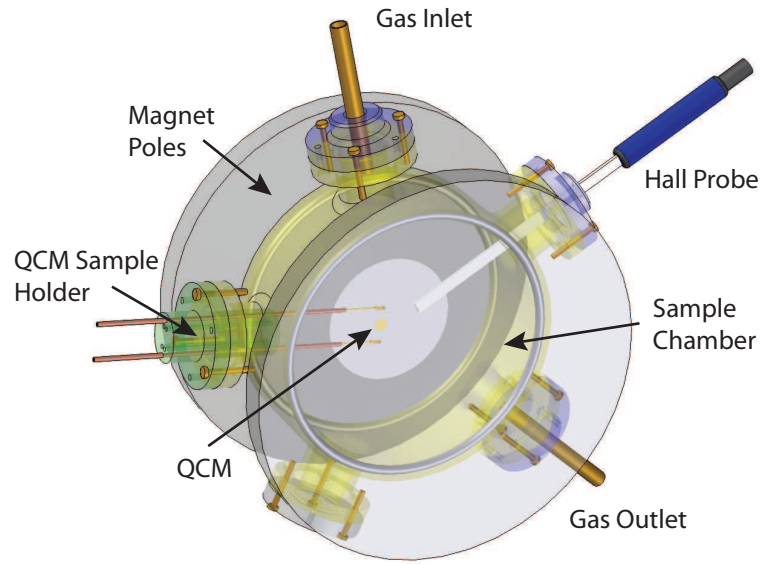
(a) Computer 3D model of MQCM sample chamber.
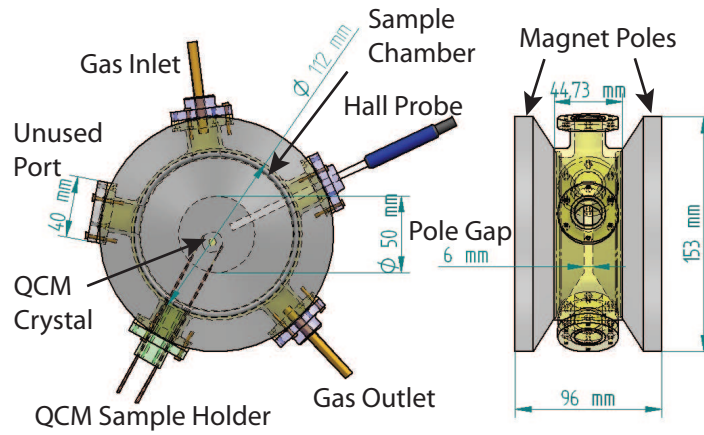
(b) Engineering drawing of sample chamber.
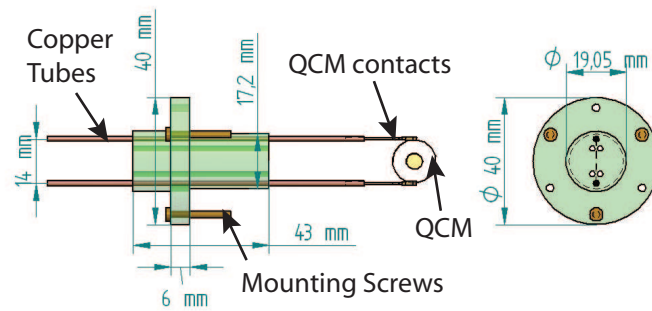
(c) Engineering drawing of sample holder.

Figure 16: Technical engineering drawings of MQCM sample chamber and holder.

on a QCM is shown in Figure 18. It is obvious from the micrograph that the cluster size of PANI is irregular. Basic film profilometry data shows that the average film roughness increases with increasing PANI concentration (Table 1). The corresponding frequency shift (df_L) resulting from mass loading for each crystal is shown in Table 1.
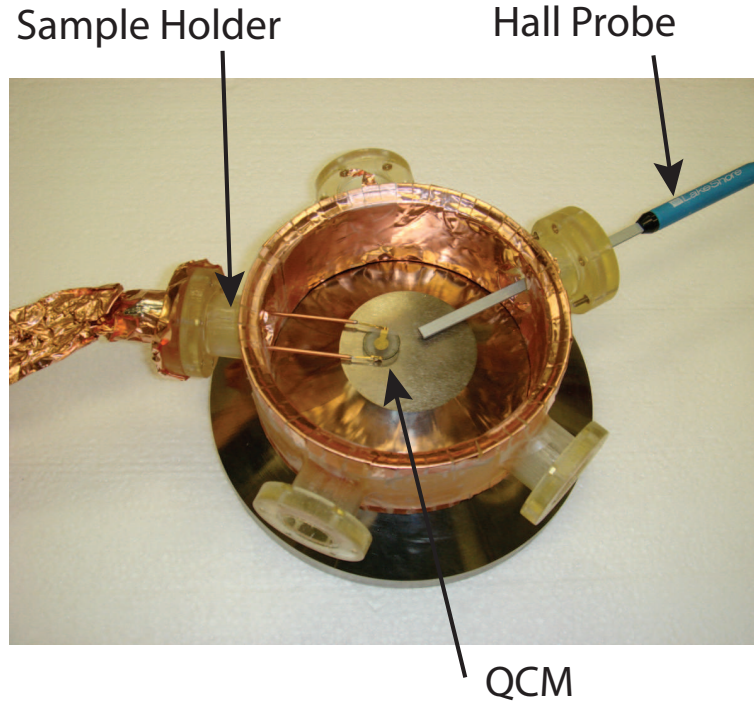
(a) Photo of the MQCM sample chamber.

(b) Photo of the MQCM sample holder.

Figure 17: Pictures of MQCM sample chamber and holder.
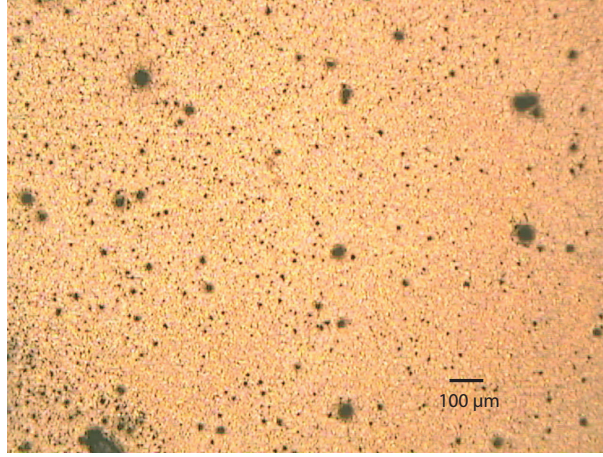
Figure 18: Micrograph of crystal 5 with 2.7%wt PANI.

2.3.2 Measurement protocol

Before and after the film deposition on the QCM, the resonance frequency and admittance were recorded. After the film deposition, the QCM was mounted on the sample holder and inserted into the sample chamber. The sample holder was connected to the oscillator, and the copper shielding was attached. The oscillator trimmer capacitor was tuned until a phase lock was achieved and further tuned to obtain the highest admittance possible. The QCM resonance frequency and admittance were continuously monitored. When the frequency drift was less than 10 Hz per hour or drifting at a constant rate, the experiment started. The experiment consisted of monitoring at the residual field for 2 minutes, then ramping up magnetic field intensity linearly for 2 minutes reaching 31 kG. Once it was reached, 2 more minutes were used to ramp down linearly to the residual field flux level and 2 minutes more of holding at the residual field. The magnetic field profile of an experiment

Table 1: Loading data from spin coat film deposition

Crystal Number	PANI Concentration	Frequency Shift (df_L)	Est. Mass Added $(0.233 Hz/ng/cm^2)$	Avg. Roughness (R_a)
1	0%wt	44.11 kHz	10.28 μg	0.5872 μm
4	1.3%wt	49.07 kHz	11.43 μg	0.9622 μm
5	2.7%wt	31.43 kHz	7.32 μg	1.1457 μm
6	5.3%wt	37.76 kHz	8.80 μg	1.9679 μm

is shown in Figure 19. The field intensity was controlled by a predetermined current-versus-field-intensity-calibration curve. That sequence was repeated at least four times for each sample.

Often, the QCM frequency had a slow near-linear drift through the experiment. The experimental results were corrected mathematically for such linear drift. The frequency was monitored until a clear linear drift was reached. The experiment began with a 2 minute period at zero current to determine the drift rate.

After all the magnetic field response measurements were completed, a further experiment was done to demonstrate the change in the magnetic properties of the PANI films resulting from acid doping. All films were placed in a closed glass container together with a small beaker with 1M HCl. After the glass container was closed, the HCl vapor diffused throughout the volume of the container, doping the PANI suspended in the PEG material for 40 minutes. This vapor-doping process produces more free electron spins in PANI, as indicated by the change of the dark blue color of PANI-EB to dark green of polyaniline-emeraldine salt (PANI-ES) [40, 41, 49]. The magnetic field response experiments then commenced.
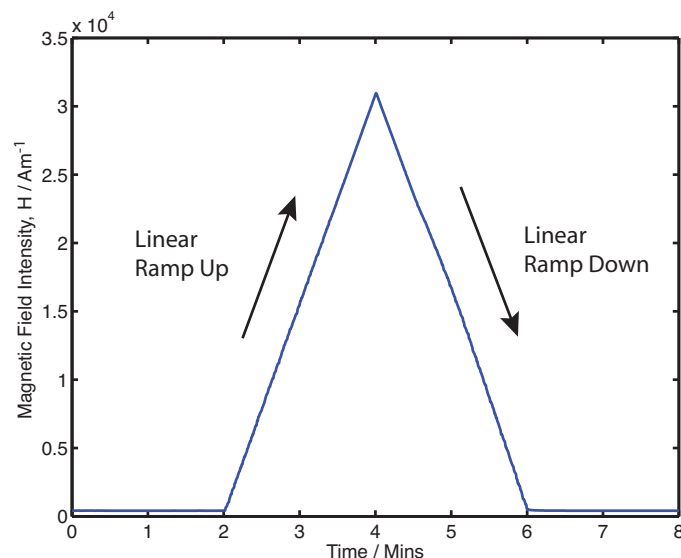
Figure 19: Magnetic field intensity profile for a typical experiment.

2.4 RESULTS

Our observations clearly show an increase of QCM resonance frequency with increasing magnetic field. Figure 20 shows the shift of QCM resonance frequency divided by the corresponding loading frequency shift (df_L) as a function of the magnetic field intensity for the different concentrations of PANI particle suspension film. The loading normalized QCM resonance frequency clearly responds to the increase of magnetic field intensity, yielding a magnetic response curve resembling an arbitrary $B - H$ curve. The higher concentration of PANI in the films produces a clear response, while the film with no PANI has almost no response. The magnitude of the response for the films with PANI appears to be doubling with PANI concentrations. There is also a clear hysteresis between the frequency shift curve for increasing and decreasing magnetic field intensity (Figure 20). It is known that paramagnetic materials should exhibit a linear $B - H$ curve, while ferromagnetic materials would exhibit a saturation curve with hysteresis. Perhaps PANI falls in between these two classes of materials. There are additional somewhat characteristic features on the response curve. However, it is premature to speculate on the exact nature of these features. Although the equivalent electrical impedance data of the QCMs were taken during the experiment, the signal was too noisy to yield meaningful information. However, the QCM impedance data acquisition will be improved in the future.

The magnetization curves of the PANI in PEG films before and after doping are shown in Figure 21. The 0 %wt PANI film showed no change to its Δf vs H curve. The curves for 1.3 %wt and 5.3 %wt PANI films show a clear increase of magnetic response magnitude with the doping. The HCl doping must have affected the PANI in the film over and above mass increase to produce such changes in Δf vs H curves. This effect would be expected as the number of free spins in PANI-ES has increased.

2.5 DISCUSSION

Interestingly, no magnetization effects have been observed in continuous films of PANI, either before or after doping. *Only suspensions of PANI particles* dispersed in PEG film

produced the magnetization effect. To explain the possible MQCM response, we have formulated two working hypotheses. The first one is called "Acoustic impedance perturbation." It is based on the idea that the externally applied magnetic field will stiffen the film by increasing the force coupling between magnetic particles. Imagine two identical small ball magnets shown in Figure 22. When they come close together, they are attracted to each other and a certain force is generated on both balls. Now, if the degree of magnetization of both magnets changes, this coupling force changes as well. Also, if the transverse (vertical) position of one ball changes in a sinusoidal fashion, the interactive force acting on the second ball will cause it to move sinusoidally, but with a reduced amplitude. In other words, the two balls behave as a *weakly magnetically coupled mechanical oscillator.* The amplitude of the second ball will be amplified by the gradient of magnetic force because of the lateral distance between them. The coupling phenomenon between these two ball magnets is analogous to particles suspended in a polymer matrix. When small particles
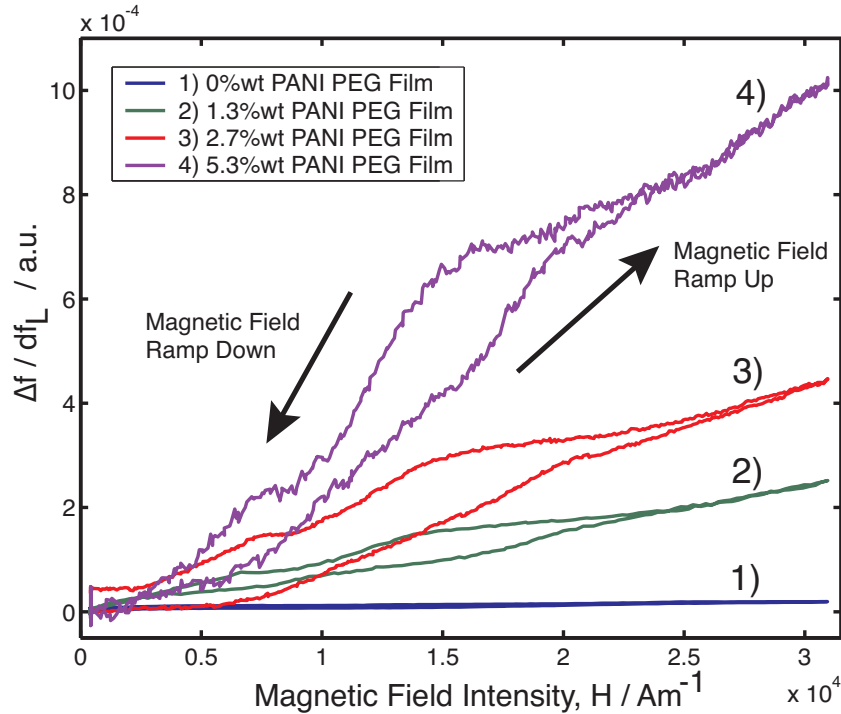
Figure 20: Comparison of the increasing delta QCM frequency ($\Delta f = f_t - f_0$) to mass loading frequency shift ($\Delta f / df_L$) ratio as a function of magnetic field sweep for the different PANI concentration in the PEG films.

are suspended in a polymer matrix as a film on top of a QCM electrode plate, the electrode shear wave motion forces them to oscillate. This effect is observed at zero magnetic field. When a magnetic field is applied , the particles couple their motion and promote the propagation of acoustic waves in the film, thereby decreasing their acoustic impedance and increasing the resonant frequency. Studies have been done on QCM and polymer melting transitions and determined that a change in material impedance without mass change will increase the QCM resonance frequency [33]. It is possible that this magnetically induced acoustic impedance also changes the resonance frequency.

The second working hypothesis relies on the motion of the particles as they propagate the acoustic wave. It is called "Magnetic disturbance hypothesis." A rapidly moving particle in the presence of a uniform magnetic field will cause a local disturbance to the uniformity of the field flux density Figure 23. This disturbance occurs because the particles create a magnetic field gradient at the interface between particle material and surrounding polymer matrix. If the particle oscillates, then the resulting field disturbance is also perturbed at
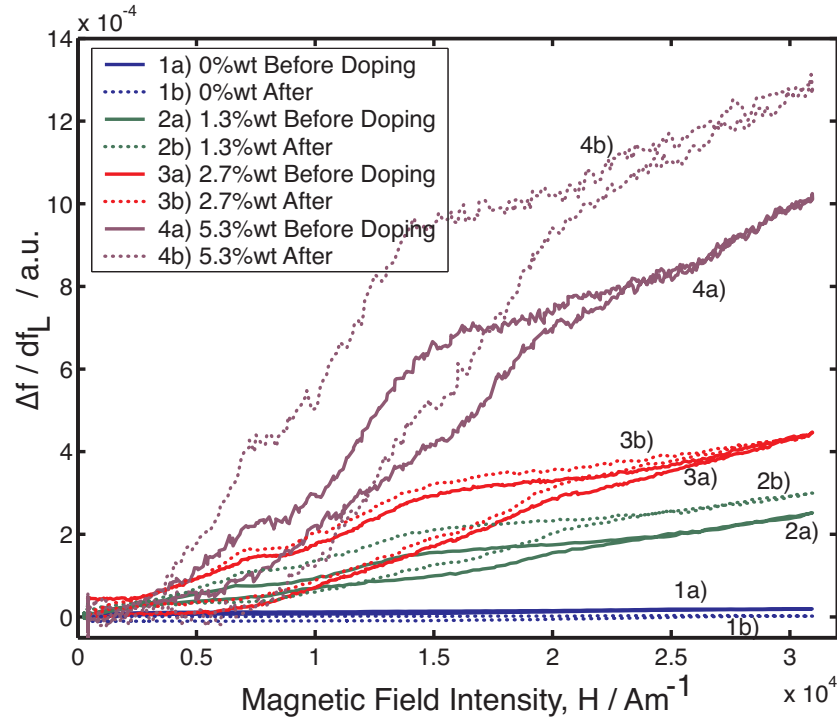
Figure 21: Response curves before and after HCl doping of the PANI PEG films.

26

the same frequency as the particle oscillations. The field disturbance can be picked up by the QCM electrodes and converted to an oscillating voltage. The oscillating voltage from the field disturbance will be in the same frequency of the electric field in the QCM. This effect is similar to the principle of the vibrating sample magnetometer (VSM) in which an induction coil converts the field disturbance to an AC voltage signal. Unlike the VSM, which oscillates at 70-200 Hz, the QCM oscillates at around 10 MHz. The coil inductance in VSM, which limits the frequency that can be picked up, does not apply to the QCM electrodes since they have much lower inductance. Therefore, it is possible that the field disturbance caused by the oscillating particles will constructively interfere with the QCM
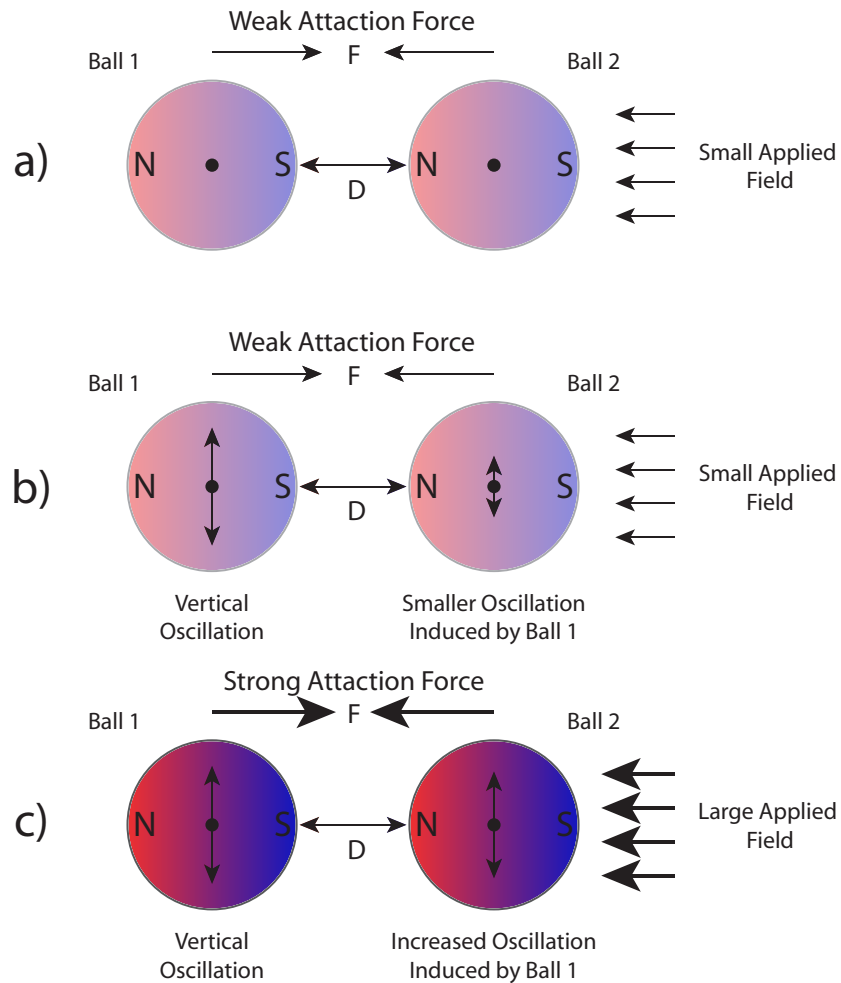
Figure 22: Diagram explaining the "Acoustic Impedance" hypothesis using "two balls" analogy a) Weak attraction force between two balls. b) Movement oscillation on ball 1 induces smaller oscillation on ball 2. c) Attraction force increased due to applied field increasing induced oscillation coupling on ball 2.

electrical oscillations. Attempts to using a network analyzer to detect this phenomenon have not yielded unambiguous results. Electrically, the network analyzer and oscillator mode of measurement are quite different. The network analyzer excites the QCM and reads the frequency response of that excitation. However, an oscillator converts the frequency response to the oscillating voltage of the QCM, amplifies the signal, and then feeds it back to the QCM. In such a case, the oscillator works as a positive feedback loop. Any electrical disturbance near the oscillating frequency to this feedback loop will change the frequency of the oscillations. If an electrical disturbance is generated from the magnetic field disturbance it may interfere with this electrical feedback loop.
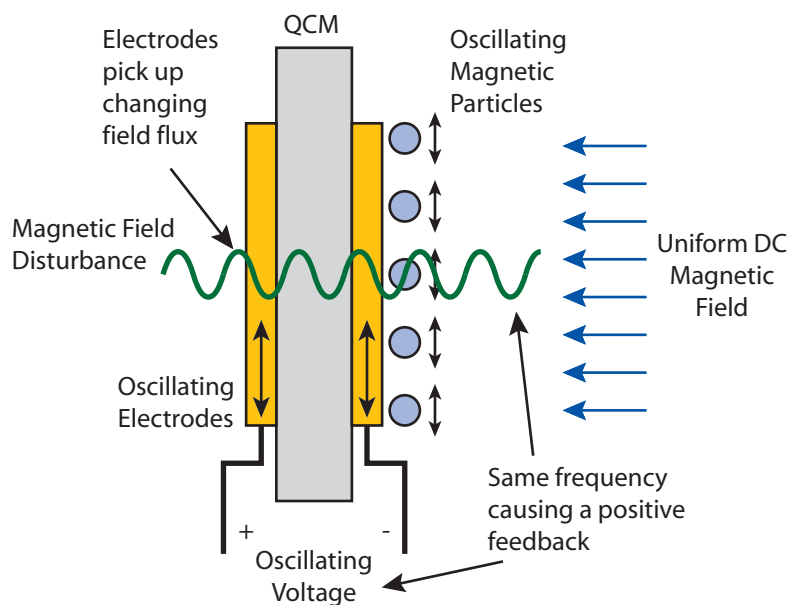
Figure 23: Magnetic field disturbance hypothesis due to moving particles in PEG films.

2.6   INTERIM CONCLUSIONS TO CHAPTER 2

Experiments have shown the new MQCM instrument can respond to magnetic properties of materials and detect the change of such properties resulting from a chemical reaction. From the results of these experiments, the MQCM instrument clearly has potential as a viable tool for the study of material magnetic properties. The promise for an in-situ magnetic

property measurement tool in a controlled chemical environment is real. However, the understanding of the mechanism, quantitative measurement, and the complete interpretation requires network analysis described in Chapter 4.

CHAPTER III

QCM PROXIMITY EFFECT

3.1 INTRODUCTION

QCMs and other acoustic resonators are commonly used as mass sensor platforms [24]. Since the first use of QCMs as a gravimetric tool by Sauerbrey [46], research surrounding the technology has been extensive. In the past, several reports have noted the influence of conductivity on the QCM when used in liquids [12, 27, 47, 57]. In 1996, M. Rodahl et al. [44] provided an explanation of the phenomenon of the liquid conductivity and influence on QCMs. Their explanation points to the additional shunt capacitance from fringing electromagnetic fields on the edge of the QCM electrodes in conducting liquids. However, through the development of magnetic QCM (MQCM) in Chapter 2 [59], we observed a new effect on highly dampened QCMs with low Q-factors. Often QCMs are mounted in flow-through cells near metal objects. In the case of MQCM, a crystal is mounted between two magnet pole faces. We have observed that the frequency shifts when these poles moves closer or further away. Further observations noted the magnitude of these frequency shifts are related to the quality factor (Q-factor) of the QCM. A higher Q-factor indicates a lower rate of energy dissipation relative to the oscillation frequency, so the oscillations die out more slowly. Under normal operation of these resonators, the Q-factor is high and the resonant frequency is not affected by external objects such as magnet poles. When the resonator is coated with an elastic sensing layer and/or operating in viscous liquids, the resonator is dampened and the Q-factor drops significantly. Under low Q-factor operation of these resonators, changes to the conductivity, proximity of the surrounding materials, as well as changes to Q-factor will significantly affect the resonant frequency. The observed QCM proximity effect seems similar to the operation principle of inductive and capacitive proximity sensors [9, 21].

Inductive and capacitive proximity sensors work as oscillating RLC resonators. By

exposing the inductive or capacitive element to a sensing target, the electrical characteristics of the material affect the exposed inductor or capacitor. A similar effect may also affect the QCM, since it can be electrically modeled (i.e. Butterworth Van-dyke Model) as a RLC resonator. External objects may alter inductive and/or capacitive values of the QCM by interaction with the fringing fields on the edge of the electrodes. The relative sizes of the electrodes and the external objects also plays a role on the fringing fields. This was described by M. Rodahl et al. [44] as a method to reduce the influence of fluid conductivity on QCM frequency. This was done by directing the fringing fields away from the liquid side of the QCM using different sized electrodes. However, simply directing the fringing fields does not remove the proximity effect.

To confirm and further study this proximity effect on the QCM, a thin disc of material would be positioned in parallel to a QCM. The distance between the disc and the QCM would be varied and the resonant frequency measured. Because the Q factor of the QCM determines the energy stored in resonance, the lower the Q factor the greater the energy dissipated to the surrounding environment. Thus, QCM with lower Q factors enhances the proximity effect. The electrical conductivity of the external material may also influence the magnitude of the effect. Disc materials with different conductivity will be used in this experiment. The final parameter in the proximity effect with QCM is the electrical connection of the external material to the electrodes of the QCM. The proximity effect exists when the external object is not electrically connected to any of the QCM electrodes. By connecting one of the electrodes on the QCM to the external conducting material, the material will further affects the fringing fields compared to a electrically floating external object.

3.2   DESIGN AND CONSTRUCTION

3.2.1   Overall experiment setup

The experiment setup for exploring the proximity effects of QCMs consisted of a single QCM, network analyzer, oscillator, frequency counter, relay circuit, data acquisition card, and a custom made mechanical stage. The setup diagram is shown in Figure 24.

31

The QCM was a 13.67 mm diameter 10 MHz AT-cut quartz crystal with 5.1 mm diameter electrodes manufactured by International Crystal Manufacture Inc. The electrodes are made of 100 nm of Au on top of 10 nm of Cr for adhesion to the quartz.

A Maxtek PLO-10i QCM oscillator was used with the QCM. The oscillator output the frequency via an analog sin wave. The QCM frequency was digitized using a HP 53131A frequency counter.

A HP E5100A Network Analyzer was used to acquire the magnitude and phase responses of the QCM. The network analyzer was calibrated using the 1-port/3-term method.

A small mechanical relay switching circuit was built to switch the electrical configuration of the experiment. Two relays connected to each of the QCM electrodes can be electrically shorted with the proximity disc upon signals from digital outputs on a data acquisition card. The data acquisition card used is a National Instruments PCI-6259 with a SCB-68 terminal box.

3.2.2 Mechanical setup

A specially designed fixture was built to hold the QCM and to allow repeatable positioning of objects relative to the QCM. The setup also allowed electrical connection to both electrodes of the QCM and to the positioned object and also variation of the Q-factor (Figure 25). The QCM was held between two o-rings. The top side opened to air and the disc of external material. The bottom side contacted the damping fluid to control the Q-factor of the QCM by the viscosity of the fluid. The electrical contacts to the QCM were made of a gold
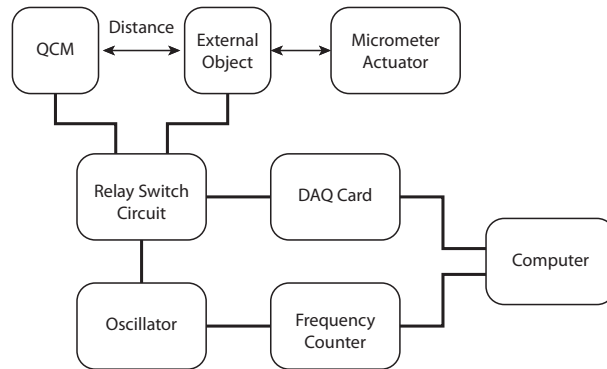
Figure 24: Diagram of the QCM proximity experiment setup.

plated clip extracted from a wire-wrap IC dual in-line package (DIP) socket. The contacts were fitted into a holder and the holder was inserted into a slot parallel to the QCM. The electrical contact was made by small mechanical pressure. The disc of material was held in place by a vacuum suction tip shown in Figure 25. A thin copper wire in the form of a spring was inside the vacuum suction tip but protruding out of the tip. If a disc was held at the tip, the copper wire will contact the disc creating a electrical connection. A brass tube on the side of the vacuum tip served as plumbing connection to the vacuum pump and electrical connection to the disc of material. The vacuum suction tip was actuated by a Starrett 463MP micro-meter and guided by four shoulder screws. Springs were used to provide opposing force to the micrometer actuator. Several set screws were used to set the micrometer in place so that 0 mm on the micrometer approximates 0 mm from disc to QCM. The distance calibration was made by adjusting the position the micrometer at 0 mm reading until electrical contact was made to the QCM electrode.
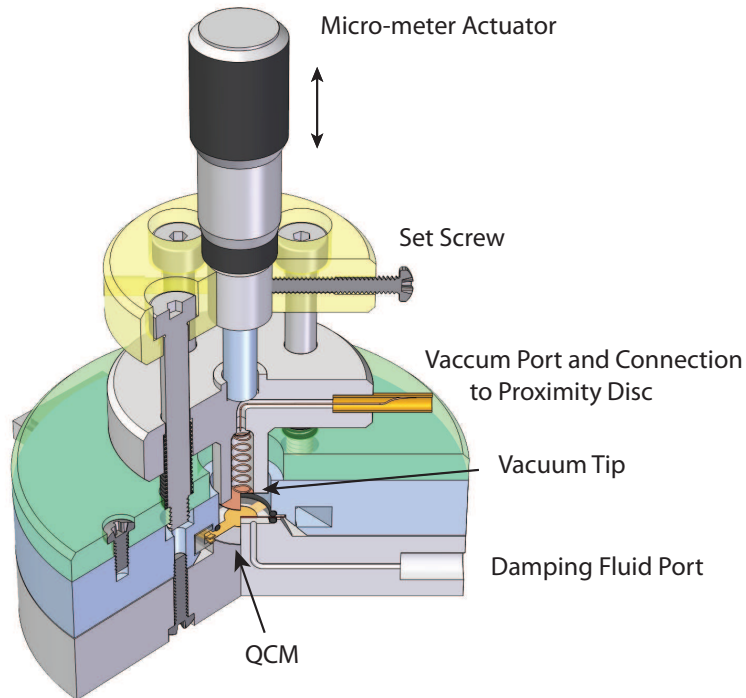
Figure 25: Mechanical setup for the QCM proximity experiment.

3.3 EXPERIMENT

3.3.1 External objects

Three different object materials; polyvinyl acetate (PVA), nickel, and copper were used to examine the effect of material conductivity and proximity to the QCM. These materials were punched from a foil into a circular disc of 7.14 mm diameter then flattened using a press. The discs have a thickness of 0.1 mm. These discs can be electrically connected to either electrode of the QCM. There are three electrical configurations we used in our experiments; floating, short-to-proximal, and short-to-distal. The floating configuration shown in Figure 26a. was when the disc is not electrically connected to any of the QCM electrodes. The short-to-proximal configuration shown in Figure 26b. was when the disc is electrically connected to the QCM electrode nearest to the disc. The short-to-distal configuration shown in Figure 26c. was when the disc is electrically connected to the QCM electrode furthest to the disc.
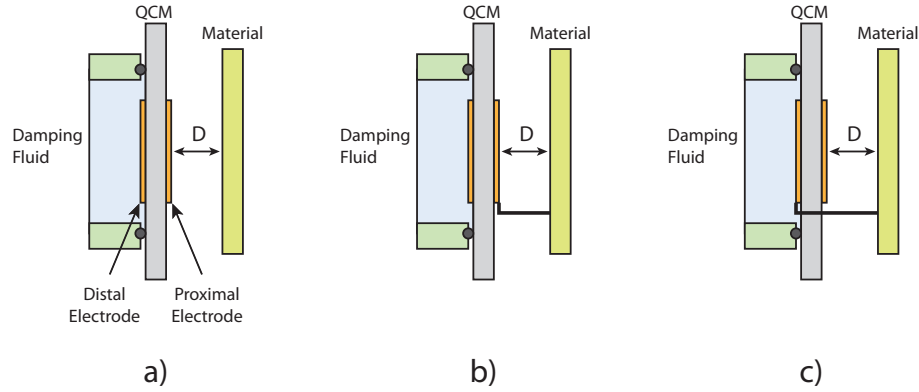
Figure 26: Three different electrical configurations of external disc and QCM electrodes. a) floating b) short-to-proximal c) short-to-distal

3.3.2 Damping fluids

It is known that viscous fluids can dampen the oscillations of the QCM [11, 24]. Damping fluids were used to conveniently lower the Q-factor of the QCM without removing the QCM from its housing. Four different fluids were used, air, de-ionized water, 20 %wt poly(ethylene glycol) (PEG) in water, and 40%wt PEG in water. Magnitude and phase frequency responses were taken using the network analyzer. Quality factors calculated are

Table 2: Damping Fluid Q-factors

Air	6533
DI Water	1375
20%wt PEG	602
40%wt PEG	469

shown in Table 2.

3.3.3 Experiment protocol

On the experiment setup seen in Figure 25, each experiment begins with the vacuum tip at the highest position. One of the discs was moved directly under and in line with the tip opening. Suction was turned on to hold the disc to the tip. The micrometer was then adjusted to 10 mm and the QCM frequency was monitored to ensure stability. Once the QCM frequency reached stable value with less than 1 Hz of drift per minute, the first reading was taken at 10 mm distance. The frequency acquisition sequence controls the relay circuit to measure the QCM frequency with floating, short-to-proximal, and short-to-distal electrode electrical configurations shown in Figure 26. The micrometer was decremented by 0.5 mm and QCM frequency measurement was acquired for that distance. The process was repeated until the disc was at 1 mm, then the decrement steps changed to 0.2 mm. The last frequency reading was taken at 0.2 mm. This protocol was repeated for different disc materials and different damping fluids.

3.4 RESULTS

The first set of results shown in Figure 27 explored the proximity effect for different electrical configurations and several values of Q-factor. The delta frequency on the y-axis was calculated by subtracting the initial frequency at the 10 mm distance. The two higher Q-factor results from air and water damping fluids showed a sharp decrease in the QCM resonant frequency as the copper plate approaches the QCM closer than 1 mm. As the Q-factor decreased from air to water damping fluid appears to slightly amplify the frequency decrease but also appear to increase the frequency at distances greater than 1 mm. The two very lower Q-factor results from PEG solution damping fluids caused the curves to differ from

the higher Q-factor ones by increasing the frequency instead of decreasing. With respect to electrical configuration the differences appears only in the lower Q-factor results.
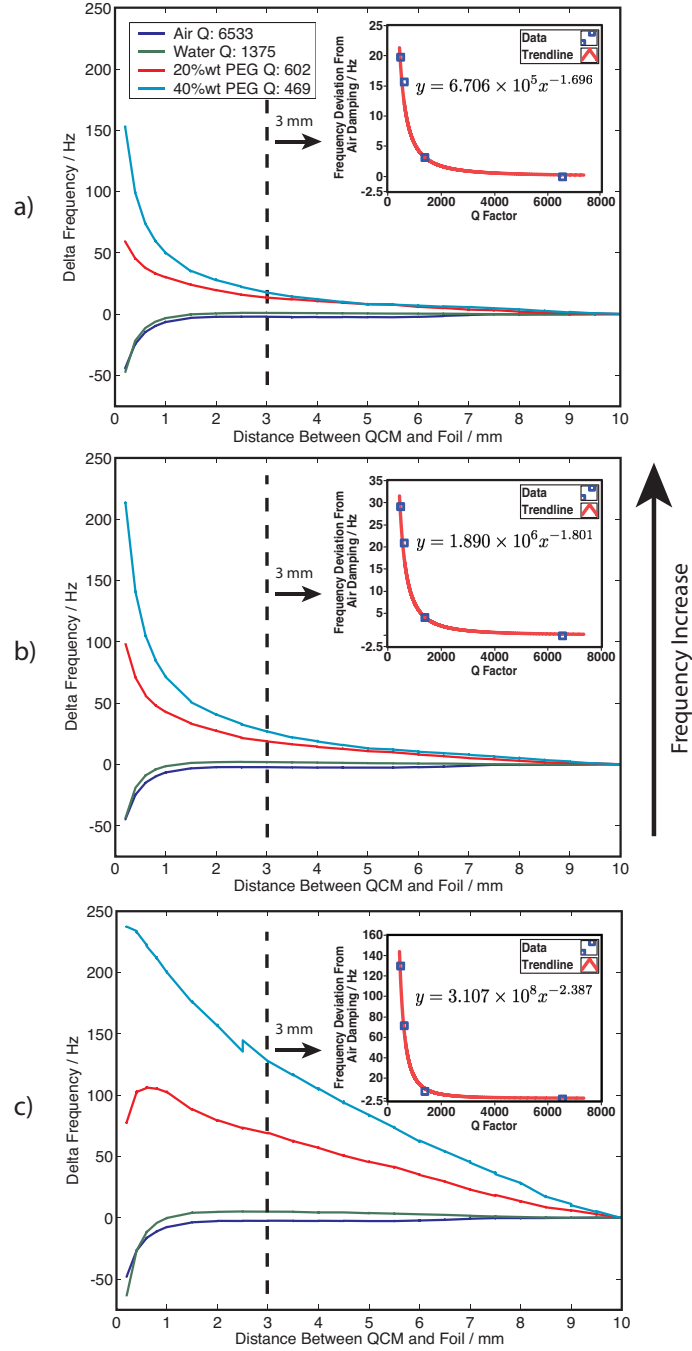
Figure 27: Comparing the effect of Q-factor for different electric configurations on the proximity effect. Subplots show the delta frequency data and trendline when compared to air damping at arbitrarily chosen 3 mm distance. a) electrically floating disc b) shorted to distal electrode c) shorted to proximal electrode.

The comparison between the different electrical configurations was illustrated in Figure 28 under a specific set of conditions described in the figure caption. Curves from floating and short-to-distal electrode configurations appears to be very similar, though the latter configuration has a greater magnitude. The short-to-proximal electrode configuration appeared to be have a greater magnitude and more importantly a different curve shape than the other configurations. From these results, the proximity effect appeared to affect the QCM at much greater distances for the short-to-proximal electrical configuration.
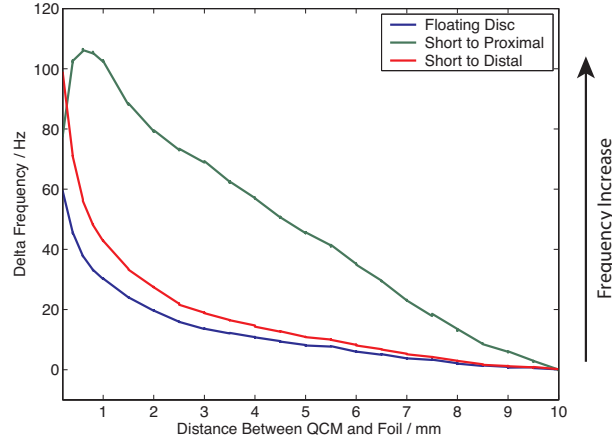
Figure 28: Comparing electrical configurations for a the case of copper disc with 20%wt PEG damping fluid.

The another set of results illustrated the effect of different plate material on the proximity effect. Figure 29 shows the different materials under a specific Q-factor and electrical configuration. The magnitude of the curves showed the increase in magnitude with the increase in electrical conductivity of disc material.

3.5 DISCUSSION

The results have clearly shown that a QCM operating in low Q-factor regime will experience proximity effects much like the inductive and capacitive proximity sensors. We believe such effect is attributed to the fringing electromagnetic fields on the edge of the electrodes. When compared with a type of capacitive proximity sensors that use fringing fields (Figure 30) [9], there is a great deal of similarity to the effect described in the results. Basic electrostatic modeling shown in Figure 31 was done in Comsol finite element modeling program to

illustrate these fringing fields. As illustrated in Figure 31, an electrically non-homogenized environment surrounding the QCM will alter the fringing field lines. In the floating disc model, the disc is bending the fringing electric field lines and moving the field density closer to the disc. In the short-to-distal model, the electric field lines are bending closer to the disc than the floating model. The disc have also created a great field density between the proximal electrode and the disc. This is expected as the proximal electrode and the disc have an applied voltage between them. However, both floating and short-to-distal cases have similar fringing field near the object. This would explain the similarities between the experiment results for those cases. The short-to-proximal electrode model shows a different bending of the fringing fields compared to other two configurations. In this configuration, the disc is attracting a greater amount of electric field that was a part of the fringing field between the electrodes. The object would cause a more pronounced effect on the fringing fields, which would explain the much greater magnitude in the experiment result.

A simple modified BVD model (Figure 32) similar to the one used in [44] can be used to describe the frequency trends from the proximity effect. Two capacitors C_d and C_p represents the fringing field capacitance from the object to the distal and proximal electrodes respectively. As the distance between the object and the QCM decrease, the fringing capacitance will also decrease (Figure 30) [9]. By decreasing the combined C_d and C_p capacitance in that branch, the total capacitance of the BVD circuit will decrease and the resonance
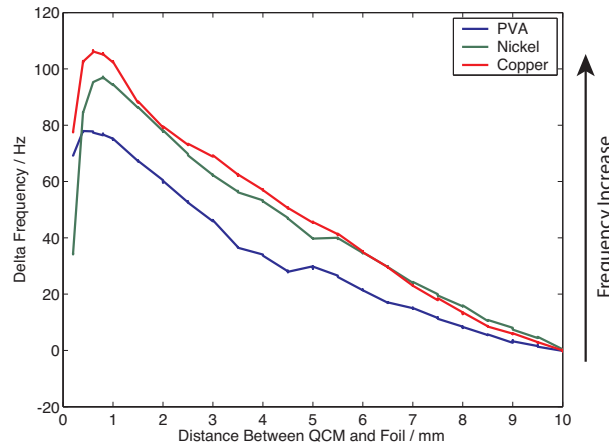
Figure 29: Comparing different disc materials for the case of 20%wt PEG damping fluid and shorted to proximal electrode configuration.

frequency will increase. However, this only explains the increase in frequency from the lower Q-factor results. The reason(s) behind the decrease of frequency at <1 mm for the higher Q-factor results are still unknown.

3.6 CONCLUSIONS

Moving objects that disturb the fringing fields will induce a frequency shift on the QCM. Exactly how much frequency change a QCM will experience depends on a great number of parameters and requires more accurate modeling. This type of effect is important because of the potential to generate frequency artifacts in QCM sensing applications. The subplots in Figure 27 demonstrate the potential impact of these artifacts. Assuming there is a 3 mm gap between the wall of the flow cell and a QCM operating in the low Q-factor regime. An injection of analyte may change the Q-factor of the QCM by either mass uptake or changes to sensing layer elasticity. In cases like this, the frequency would increase due to the change in Q-factor in addition to changes from addition of mass and rigidity as most would commonly expect. Frequency changes due to the proximity effect can easily be mistake for response to analyte. More over, if the analyte changes the dielectric constant of the solution, that would alter the fringing capacitance and would translate into a frequency shift without actually changing the mass of the sensing layer. Certainly, this type of artifacts are not be limited to QCM, mass acoustic sensing devices such as SAW and others would behave similarly to proximity of surrounding objects. In light of the high potential for measurement
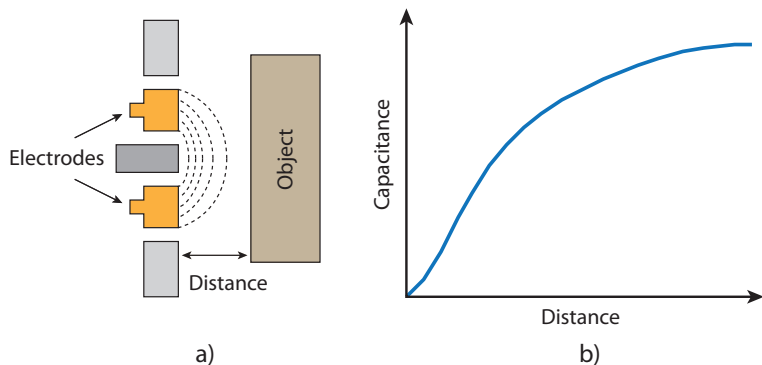
Figure 30: Basic concept of a fringing capacitive proximity sensor [9]. a) Electrode configuration and orientation to object b) Typical relationship between capacitance and distance.
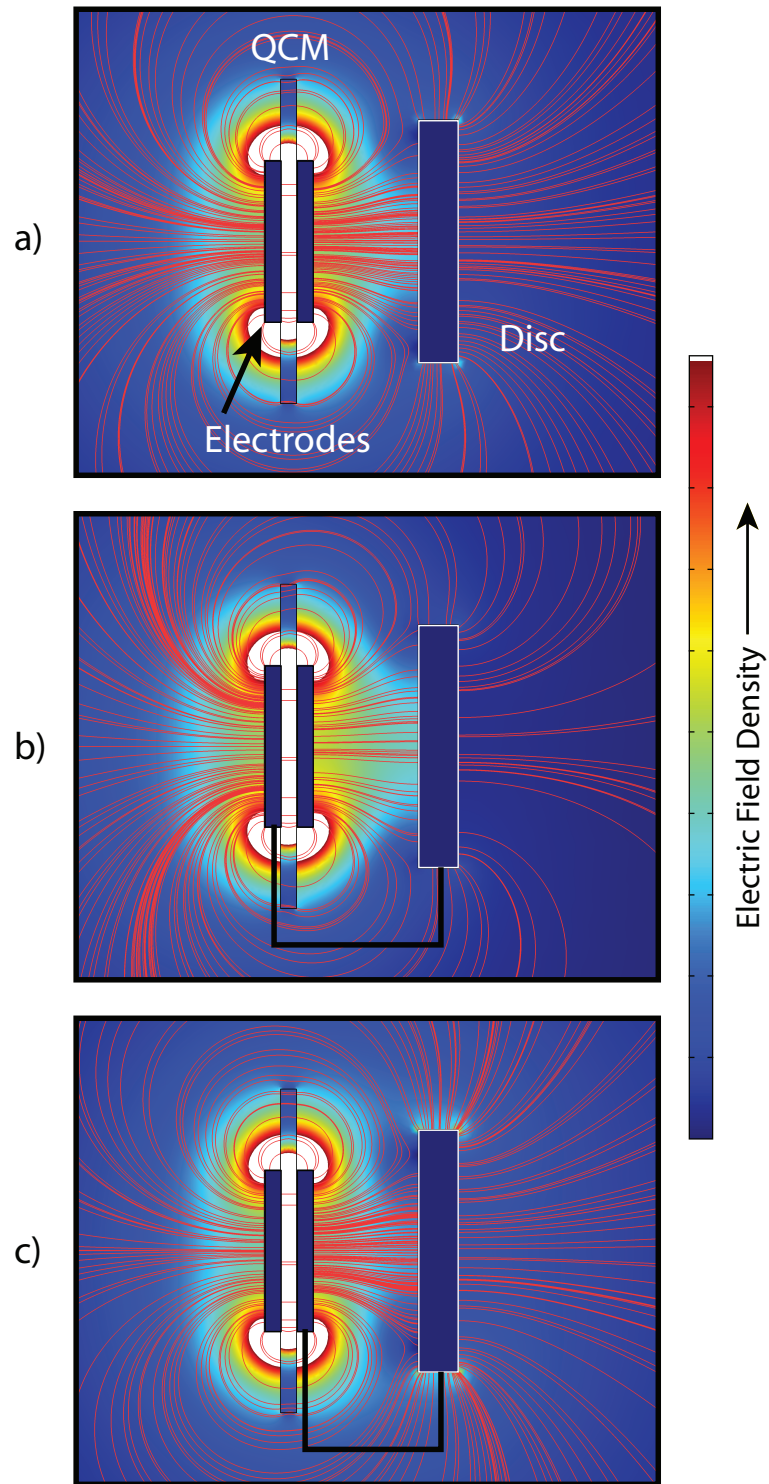
Figure 31: Basic electrostatic modeling of the electric field density (colors) and field lines. The white areas have electric field density exceeding the color intensity range. a) electrically floating disc b) shorted to distal electrode c) shorted to proximal electrode.

artifacts when operating QCMs in low Q regimes, we believe that electrical and physical size considerations must be made when designing flow-through cells for low Q-factor mass acoustic devices. Have a good reference sensor with similar Q-factor would help identify the artifacts. However, the best way to avoid potential artifacts is to operate QCMs in the high Q regime ($>$1000).

The QCM proximity effect existed in the first version of MQCM. With only 4 mm gap between the magnet poles, the QCM frequency was observed to shift ($<$ 10 Hz for 2 T of field) with applied magnetic field even when there was only diamagnetic material on the electrode to lower the Q factor. In the MQCM case, the fringing fields were influenced by the magnetc poles and further modulated by the much greater DC magnetic field. For MQCM, the influence from the proximity effect did not change our conclusions in Chapter 2. In Chapter 4, the pole gap was increased to 25 mm. With a greater pole gap, the proximity effect was reduced to less than 0.2 Hz for 2 T of field flux.
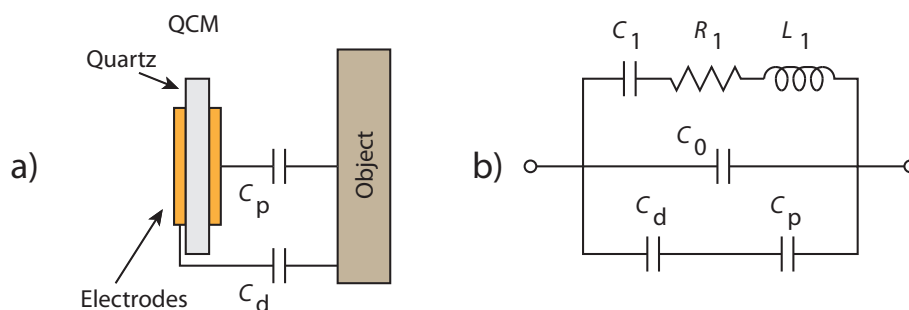
Figure 32: Modified BVD model describing QCM proximity effect. a) Relationship of C_d and C_p to the object b) Relationship of C_d and C_p to the BVD model

CHAPTER IV

MQCM: MULTI-LAYER STACK

4.1 INTRODUCTION

4.1.1 MAGNETIC MULTI-LAYER

Single and multi-layers of ferromagnetic and diamagnetic materials have been studied in conjunction with surface-acoustic-wave (SAW) devices in [20, 36, 53–55] which some call magnetic SAW (MSAW). MSAW devices were designed as tunable transmission delay lines with magnetostrictive materials which can be attenuated using magnetic field [20]. Milewski et. al [36] have found that a multi-layered configuration of magnetostrictive materials and non-magnetic materials enhances MSAW performance. However, this technique never really took off because of the small tunable attenuation range of typically around 0.001 percent.

4.1.2 MQCM CONCEPT

The first Magnetic QCM instrument was developed with the goal to use a QCM to measure in-situ magnetic properties of conducting polymer thin films during exposure to various chemicals gases [59]. We quickly realized that the MQCM instrument had potential uses in other aspects of fundamental materials related research. One area is to study the MQCM behavior with a stack of alternating ferromagnetic and diamagnetic layers in hope of gaining further understanding of the physics of the observed effects.

From the MQCM experiments in Chapter 2 with continuous homogeneous magnetic film and with magnetic particles dispersed in a non-magnetic matrix [59], we realized that the stresses between the ferromagnetic material and the diamagnetic matrix can play a role. The presence of diamagnetic material between the ferromagnetic material creates large magnetic field gradients under externally applied magnetic field. The field gradient generates stress between the separated ferromagnetic material. The similar effect may exist in a multi-layer of ferromagnetic and diamagnetic thin films.

4.2 EXPERIMENTAL

Our original MQCM instrument [59] has been modified as shown in Fig. 33. The oscillator circuit has been replaced with HP E5100A network analyzer as means to acquire QCM data. A pair of magnetic field biasing coils were added to cancel out the residual magnetic field. The magnetic pole gap was increased to 25 mm after we observed the proximity effect in Chapter 3 affecting the operation of the QCM [58]. The sample chamber and QCM holder shown in Fig. 34 were also modified to provide proper electrical shielding and air tight seal.
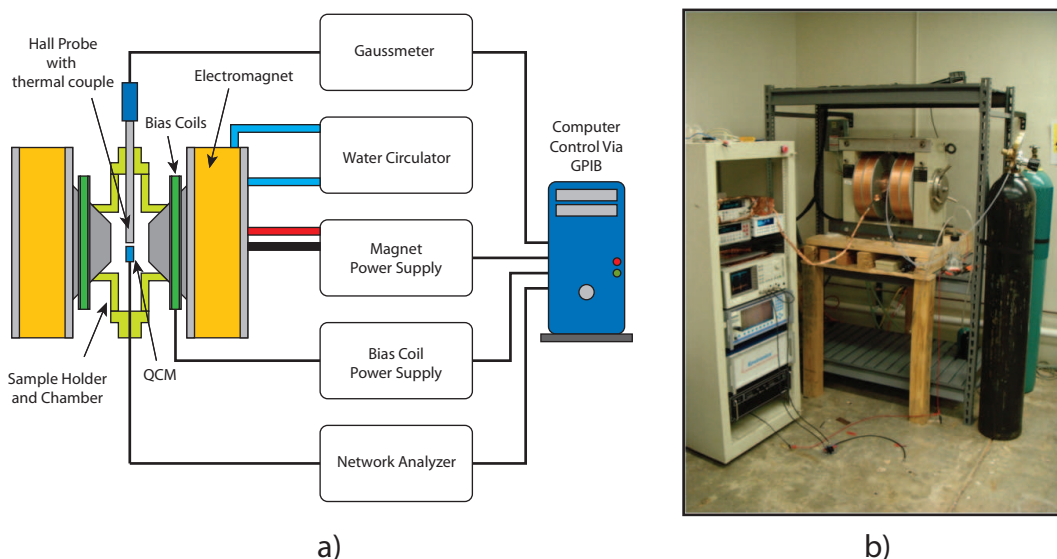

a)   b)

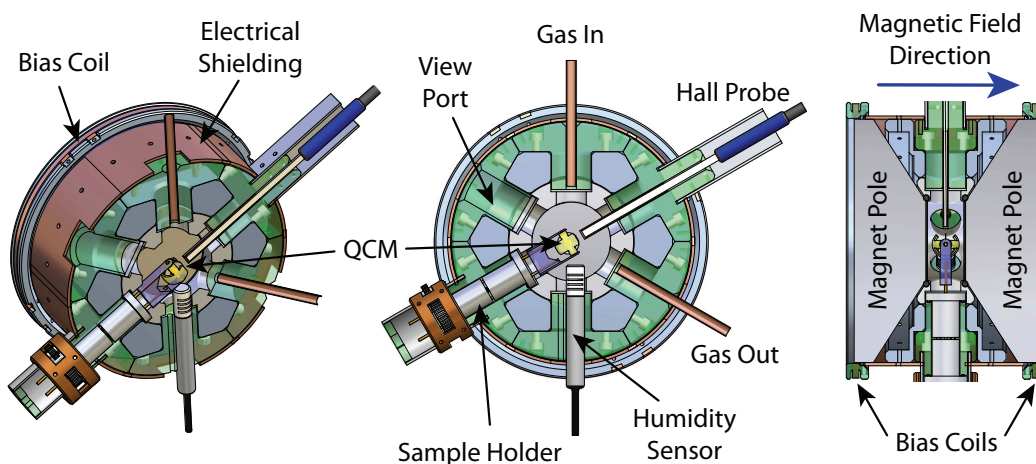**Figure 33:** Updated Magnetic Quartz Microbalance (MQCM) system diagram.

Figure 34: Engineering drawing of the MQCM sample chamber.

4.2.1 STACK PREPARATION

The crystals used in this experiment were 10 MHz QCMs from International Crystal Manufacture Inc. They have a diameter of 13.67 mm and the electrodes have a diameter of 5.1 mm with 10 nm of Ti adhesion metal and 100 nm of Au. The alternating layers of nickel and gold were deposited on a QCM electrochemically. The stack starts with a layer of nickel on the original gold electrode. The nickel electroplating solution was a "Watts bath" [61] with 22.34g of $NiSO_4.6H_2O$, 3.56g of $NiCl_2.6H_2O$, and 3.58g of H_3BO_3 in 100 ml of water then diluted one to ten with de-ionized water. The deposition of gold was done from the bright electroless plating solution(Tranesene Inc.) Although the gold plating solution is an electroless plating solution, it can be used as a electroplating solution at room temperature. The electroplating was done in a three-electrode configuration with working, counter, and reference electrodes. The reference electrode was Ag/AgCl, 1 M KCl // 1 M KNO_3. For the nickel depositions, nitrogen gas was bubbled through the plating solution for five minutes to minimize formation of nickel oxide. The plating process was done by sweeping the potential from 0 V to -1.4 V at 20 mV/s for nickel and 0 V to -1.2 V at 40 mV/s for gold. A total of 28 alternating layers of nickel and gold were deposited. The integrated charges, calculated mass, and delta frequency of the QCM for electroplating each layer is shown in Fig. 35. The entire stack was created in three steps. The first stage created 12 layers; six nickel and six gold layers. The QCM was then heated to 150°C for 16 hours to anneal the layers. MQCM measurements were taken and eight additional layers were added for a total of 20 layers. The 20 layered stack was then annealed at 150°C for 16 hours. MQCM measurements were taken and eight more layers were added for a total of 28 layers. After another anneal, MQCM measurements were taken. Each MQCM measurement resulted in exposure of the stack up to 10,000 Gauss magnetic field. For comparison, another QCM was used to deposit ten consecutive nickel layers then ten consecutive gold layers achieving similar total mass of nickel and gold to the 20 layer alternating layered stack. This QCM was also annealed at 150°C for 16 hours.

4.2.2 MQCM MEASUREMENT

The MQCM measurements were done using a HP E5100A network analyzer. The network analyzer was calibrated using the 1-port/3-termination method. The QCM admittance was measured using the network analyzer. It was set to 1600 points per 500 ms sweep for a narrow bandwidth centered around the resonance frequency. After the QCM was mounted into the holder, electrical connections were checked by observing the peak on the admittance magnitude and the phase curve. The QCM was kept under atmospheric pressure in air and room temperature. After stable reading was reached, the magnetic fields of approximately 0 Gauss (G) , 1kG, 3kG, and 10kG were applied to the QCM. At each field value, 20 sweeps on the network analyzer were averaged and recorded.

4.3 *RESULTS*

The results from the 12 layered stack are shown in Fig. 36. The admittance magnitude of the 12 layered stack at the resonance peak increases slightly with respect to magnetic field in Fig. 36a. The phase also shifts slightly in Fig. 36b and the narrower frequency span Fig. 36c. Eight more layers were then added to the 12 layered stack, the resulting MQCM measurements are shown in Fig. 37. The admittance magnitude clearly decreases with increase of magnetic field. The admittance phase decreases left of the maxima frequency and increases to the right of the maxima frequency with increase of magnetic field. Another
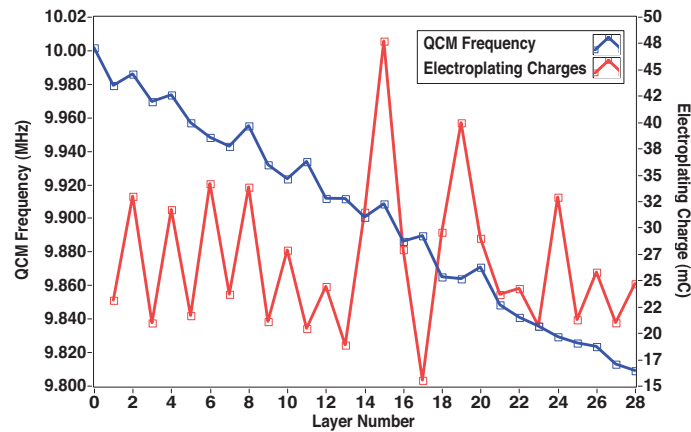
Figure 35: Frequency of QCM and charge for each electroplating layer.

eight layers were added in addition to the existing 20 layers. The resulting MQCM measurements are shown in Fig. 38. Similar to the MQCM results from the 20 layered stack, the admittance magnitude clearly decreases with increase of magnetic field. However, the decrease in magnitude from the 28 layered stack is greater than the 20 layered stack. The phase shift pattern for the 28 layered stack is also similar to the 20 layered stack, but more pronounced. The MQCM data was re-plotted in Fig. 39a by taking the percentage change of the maximum admittance from zero magnetic field. From the phase data, the zero phase frequency is re-plotted in Fig. 39b. As seen in Fig. 39, it is clear that both admittance magnitude and zero phase frequency follows a saturating curve with respect to magnetic field. Such curves are typical of ferromagnetic materials.

The second QCM with consecutive nickel and gold layers used for comparison showed negligible changes with respect to magnetic field.

4.4 DISCUSSION

MQCM measurements of alternating multi-layered ferromagnetic nickel and diamagnetic gold clearly show perturbation with respect to magnetic field. The BVD model was used to predict a similar type of change on the admittance magnitude and phase curves. By changing the equivalent R_1 resistor in the BVD model, a similar effect to the magnetic field can be observed. The admittance magnitude and phase of a standard BVD model with L_1=584.2 μH, C_1=0.441 pF, C_0=241 pF, and multiple R_1 values is shown in Fig. 40. Comparing the curves from the BVD model in Fig. 40 to the MQCM result of the 28 layered stack in Fig. 38, the similarity is unmistakable. Change of no other equivalent parameter in the BVD model could reproduce the observed experimental results. Therefore, the R_1 component in the BVD model appears to be the representation of a QCM which is likely perturbed by magnetic field.

The R_1 component is attributed to energy losses from viscous effects and/or from internal friction [24]. Since both gold and nickel are considered to be rigid materials, bulk viscous effects are unlikely. Since the continuous consecutive layers did not show any response to magnetic field, the source of internal friction losses are likely at the interfaces

between gold and nickel layers. To investigate the morphology of the nickel/gold interfaces, another QCM was used to electroplate six recessed alternating layers of nickel and gold. This was done by covering up a portion of the electroplated area with acrylic lacquer before electroplating the subsequent layer. After the step-wise electroplating was complete, the lacquer was washed away with acetone to expose the boundaries between overlapping surfaces. This way, the surface of each electroplating could be investigated using scanning
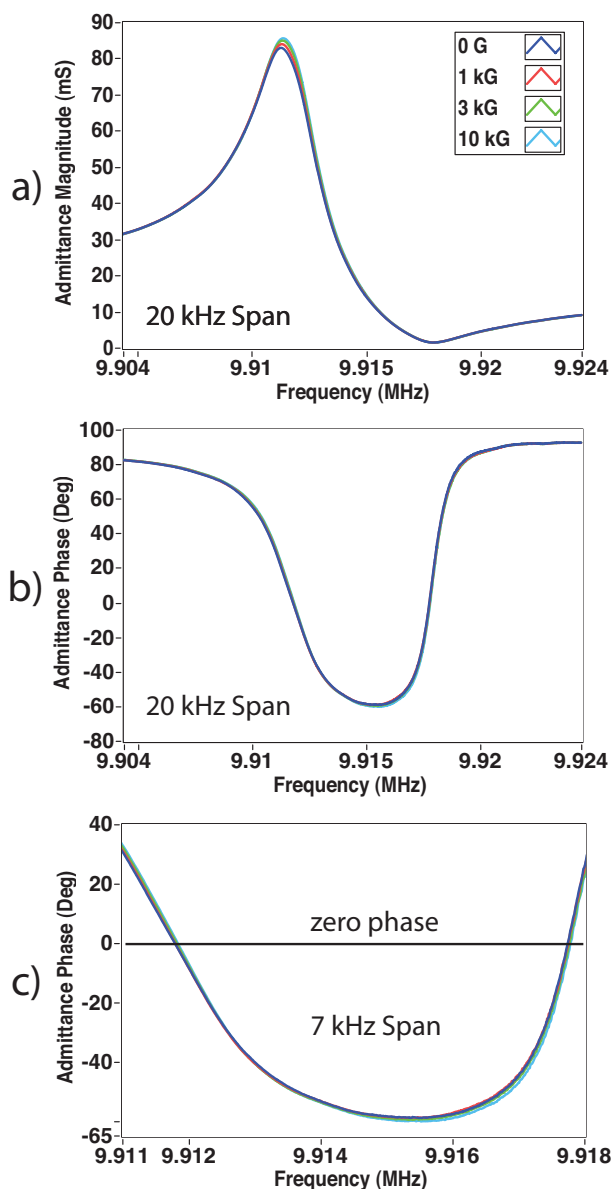
Figure 36: MQCM result of stage one with 12 layers with magnetic field shown in the graph legend.

electron microscope (SEM). Fig. 41 shows SEM pictures the surfaces of each layer taken by a Zeiss Ultra 60 SEM. From these SEM pictures, these surfaces are granular. The gold surfaces contains many grains while the nickel surfaces consist of smaller crystalline structures. We believe that these surfaces forms a interlocked boundary between nickel and gold depicted by Fig. 42. The stress of the gold/nickel boundary interlock is modulated by depth of the interlock and by magnetic field gradient acting on the nickel. For thin structures, the
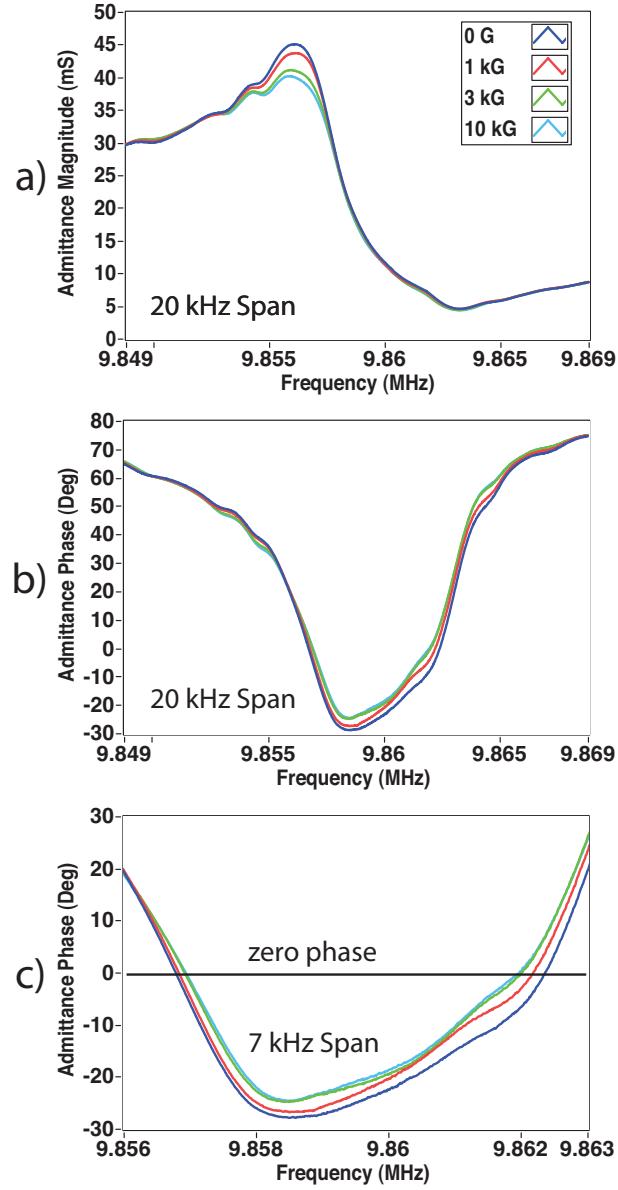
Figure 37: MQCM result of stage two with 20 layers with magnetic field shown in the graph legend.

magnetically enhanced interlock stress enhances the acoustic coupling between the layers, hence the increase in admittance magnitude with increase of magnetic field (Fig. 36). As more and more layers were added to the QCM, the structure is no longer thin and the enhanced coupling becomes a lossy acoustic component, hence the decrease of admittance magnitude with increase of magnetic field (Fig. 37,38).
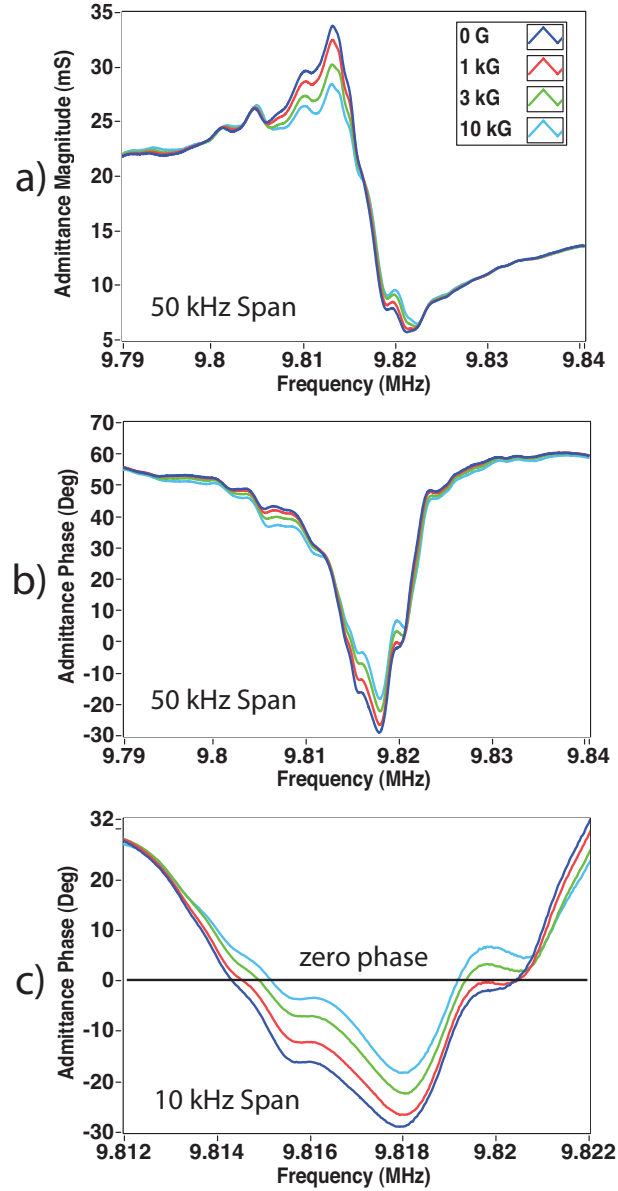
Figure 38: MQCM result of stage three with 28 layers with magnetic field shown in the graph legend.

4.5   CONCLUSIONS

We have shown that a ferromagnetic and diamagnetic multi-layered structure on a QCM exhibit changes in the admittance magnitude and phase with magnetic field is applied. From the simulated BVD model, we have shown that the changes to the QCM oscillations are due to changes in the R_1 resistor component in the BVD model.

The interfacial friction between the layers appear to be the primary source of the effect. These results underscore the importance of the morphology both at the microscopic layer level and at the level of metal grains. The possibility of giant magneto-resistance (GMR) effect has been also considered. However, the SEM images clearly do not support such possibility.
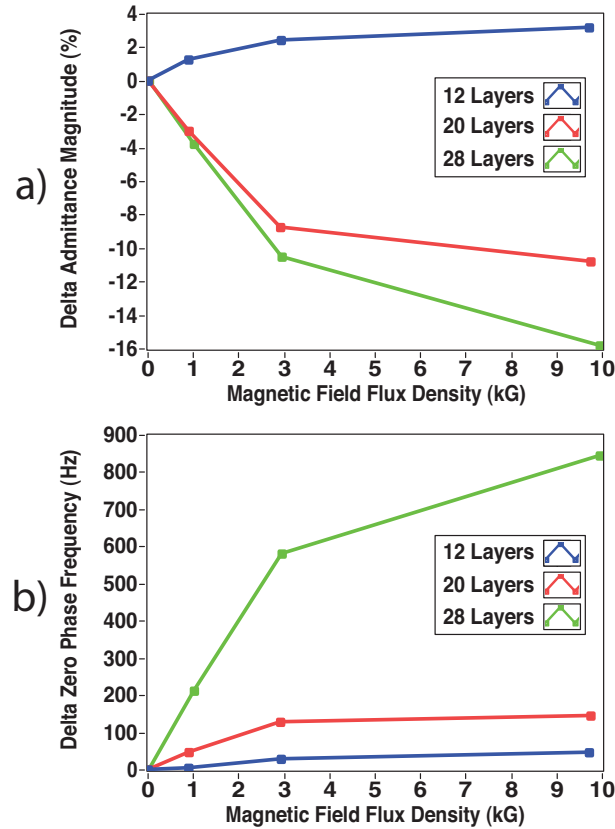
Figure 39: Delta maximum admittance magnitude in percent change from zero field and delta zero phase freq with respect to magnetic field.
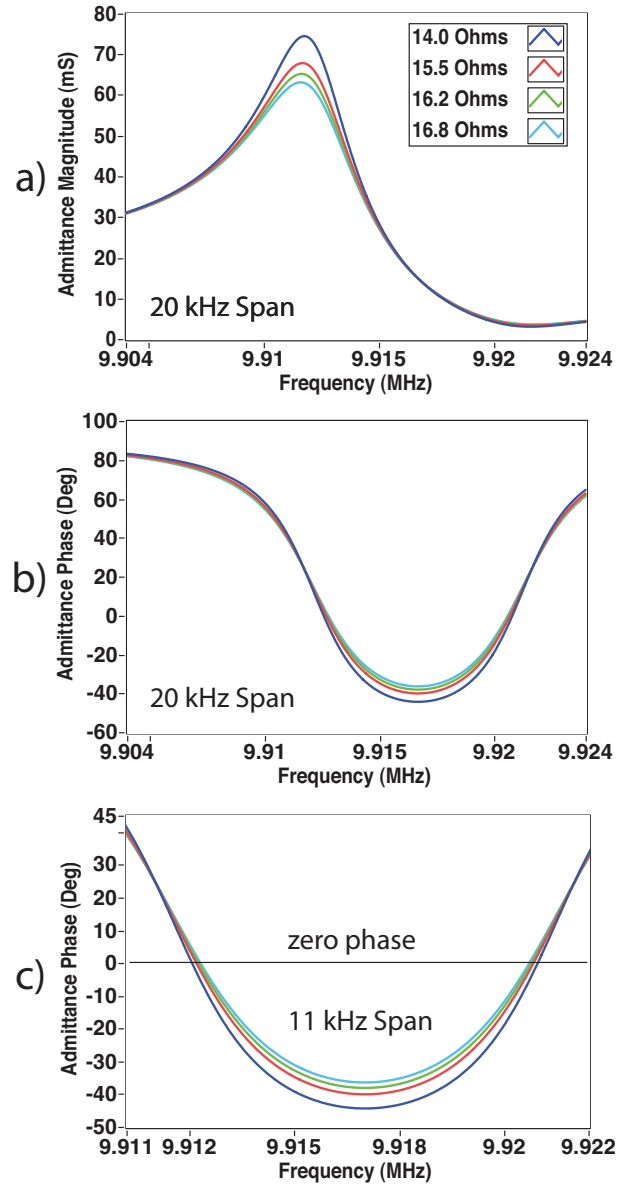
Figure 40: Simulated BVD model by adjusting R_1 component value shown in the graph legend.
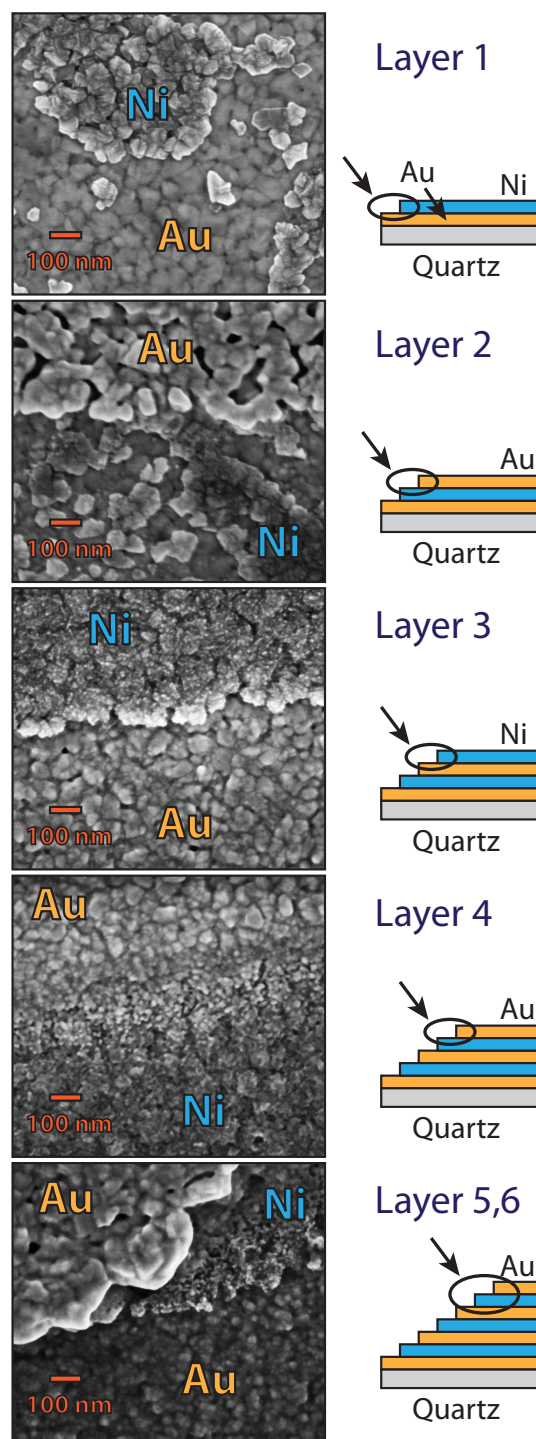
Figure 41: SEM images of boundaries between layers of a 6 layer QCM electroplated using same procedure as the 28 layered stack.
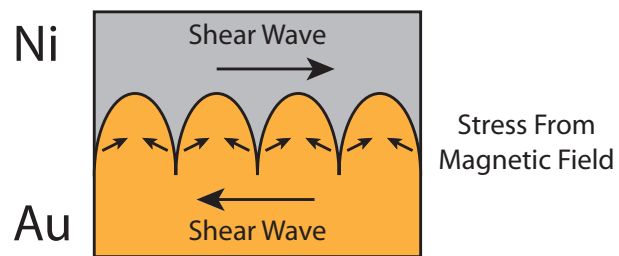
Figure 42: Cartoon of interfacial coupling due to magnetic field.

CHAPTER V

CONCLUSIONS AND FUTURE WORK

5.1 Thesis Conclusions

Throughout this project, a great deal was learned about QCMs, magnetism, and techniques to measure material magnetic properties. In Chap. 2, the first working version of the MQCM instrument was developed by using polyaniline suspension film on QCMs. The polyaniline suspension films showed clear resonance frequency shift with applied magnetic field while the continuous polyaniline film did not show any response. The frequency shift in the suspension film was also shown to increase with the chemical change in the polyaniline after HCl doping. This chapter showed that MQCM concept is valid and has the potential to measure magnetic material properties in-situ. Two transduction hypotheses were proposed. The first is based on frequency modulation by stiffening the film through magnetic field. The second is based on an analogy to VSM where magnetic field disturbance generated by moving magnetic material is modulating the QCM frequency.

During the development process leading up to the first version of MQCM, two things were learned. First, in order for MQCM to work properly and reliably, the area around the QCM and the oscillator circuit must be shielded and grounded to the electromagnet power supply. Second, the proximity of the QCM to the magnet poles or any other metal object will affect the resonance frequency. This effect is also modulated by magnetic field. The discovery of the QCM proximity effect led to the work described in Chapter 3. This chapter showed that if an object's electric permittivity disrupts the normal fringing electromagnetic field line around a QCM, the disruption will also affect the resonance frequency of the QCM. The extent of the frequency shift from the proximity effect is dependent on the Q-factor of the QCM. A simple modified BVD circuit with two additional capacitors were used to model the proximity effect on a QCM.

With the information learned from the work in Chapters 2 and 3, an improved 2nd

version of the MQCM was built. It was described in Chapter 4. In this chapter complex geometry such as particle suspension were simplified to alternating stack of ferromagnetic and diamagnetic layers. This multi-layered stack showed significant response to magnetic field, while, the two layer geometry of the same material and the same mass showed no response to magnetic field. A simple BVD circuit model shows a similar behavior by changing the resistance value in the circuit that represents frictional energy loss. Quantum effect similar to giant magnetoresistance (GMR) was considered. However, after examining SEM surface images, we realized that the sources of acoustic response to magnetic field is likely coming from material interfacial stresses and not from the quantum effects.

Overall, this thesis has opened a new research area that combines the sensitive nature of piezoelectric resonators such as the QCM and magnetic materials. The results from experiments point to the importance of interfacial stress in the transduction principle of MQCM.

5.2   Road Map Ahead

Looking ahead at the direction of work in this area, two questions need to be answered.

How do the interfacial properties between the layers in the MQCM multilayer geometry affect the acoustic response to magnetic field?   In order to answer this question the following experiments are proposed. From the work in Chapter 4, we know that concentration of electroplating bath, temperature of the bath, and electroplating voltage will affect the surface morphology of each layer. By creating QCMs multilayer stack with the same number of layers but different electroplating parameters, QCMs with smoother layer surface can be compared with QCMs with rougher layer surface. If a rougher layer surface generates a greater response to magnetic field, then that will enforces the interfacial stress hypothesis. The quality of the deposits will be monitored by SEM.

How would thickness of the layers in the multi-layer geometry affect response to magnetic field? Since the hypothesis is based on interfacial stress, then the bulk thickness of the layers should not affect the response of MQCM stack to magnetic

field. Electroplating parameters can be adjusted to create thinner layers to test the interfacial stress hypothesis. Electroplating is not the only method to create multilayered stack. Evaporation of metals as well as more complex methods such as epitaxial growth can also create very thin layers. Extremely thin (< 10 nm) single crystal layers created with epitaxy may also show quantum effects similar to the giant-magnetoresistance effect.

APPENDIX A

CLARIFICATION ON EFFECT OF MAGNETIC FIELD ON STIFFNESS AND RESONANCE FREQUENCY OF QCM

This appendix contains unpublished data. Experiments to support this theory are in progress. Nevertheless, the observed effects of increased mechanical stiffness of the PEG/PANI composite in magnetic field is well within the range predicted by (8) and supported by experimental measurement shown in Figure 43.

A.1 Magnetic Properties of Polyaniline

Polyaniline is a conducting polymer in its emeraldine state. Recent studies [8, 13, 25, 29] on the polyaniline emeraldine have shown it to be paramagnetic material. Studies on the doped polyaniline emeraldine salt compared to undoped polyaniline emeraldine base form of the polymer also revealed increased magnetic susceptibility due to doping [25].

A.2 Elasticity of Magnetic Polymers

A non-magnetic polymer matrix can be made into a magnetic material by adding particles of ferromagnetic or paramagnetic materials into the polymer matrix. By magnetizing polymers with suspended magnetic particles, the bulk elastic modulus was reported to decrease by 1-2% [43] and the energy absorbed in the bulk decreases with increased magnetic field [35]. In other words, a 15mm x 15mm x 45mm polymer bar embedded with magnetic materials will decrease in stiffness with the application of a magnetic field. However, other polymeric magnetic composite materials studied have shown increase in stiffness with applied magnetic field [15, 60].

A.3   Relationship Between Elasticity and QCM Resonance Frequency

QCM frequency can be accurately predicted by Sauerbrey equation. However, since the Sauerbrey equation assumes the addition of material is an extension of the vibrating quartz, the equation is limited to thin and rigid films. When, an elastic film such as poly(ethylene glycol) is on a QCM, the film elasticity in addition to mass must be accounted in the resonance frequency shift. The Hunt equation (8) derived in [19] using time-dependent perturbation theory shows the role of elasticity change in shear modulus, $(\Delta\mu)$, on affecting resonance frequency shift in a QCM. In this equation, $\Delta\omega$ is the change in QCM resonant frequency in radians, $\Delta\rho$ is the change in mass on the QCM, V_s is the acoustic velocity in AT-cut quartz, ω_u is the fundamental frequency of the QCM, $\sqrt{\rho_q\mu_q}$ represents the acoustic impedance in the quartz, and h_f is the thickness of the elastic film on the QCM. The Hunt equation (8) is very similar to the well-known Sauerbrey equation but with the additional term $\frac{\Delta\mu}{V_s^2}$ to account for static changes to the mechanical stiffness of a film on a QCM. This equation points out that addition of mass to a QCM will lower the resonant frequency, but an increase in film stiffness will actually increase the resonant frequency.

$$\Delta\omega = -\frac{\omega_u^2 h_f}{\pi\sqrt{p_q\mu_q}}\left[\Delta\rho - \frac{\Delta\mu}{V_s^2}\right] \qquad (8)$$

A.4   Estimation of Shear Stiffness via QCM Frequency Shift Due to Magnetic Field

The Hunt's equation (8) can be used to reverse the calculation of frequency shift to instead calculate change in shear stiffness $\Delta\mu$. The term $\Delta\rho$ can be removed since in MQCM measurements, the mass of the film remains constant. With $\Delta\rho$ removed, (8) can be rewritten with $Z_q = \sqrt{\rho_q\mu_q}$ as

$$\frac{2\Delta f Z_q V_s^2}{(2\pi f_q)^2 h_f} = \Delta\mu$$

For the case of the MQCM and Polyaniline suspension in Poly(ethylene glycol), the f_q frequency is 10 MHz, Z_q is a well known constant for AT-cut quartz at $8.8 \cdot 10^6 kg \cdot$

$m^{-2}s^{-1}$. The acoustic velocity of the quartz, V_s, is a constant at $3.34 \cdot 10^4 m/s$ and film thickness is assumed to be around 10 μm. With the constants, the Hunt equation can be reduced to a simple linear scalar. The $\Delta\mu$ can be calculated from the Δf results from Chapter 2. Figure 43 shows the raw delta frequency measured in MQCM with undoped Polyaniline/PEG composite. Scaling figure 43 with the reduced Hunt equation results in Figure 44 showing the calculated $\Delta\mu$ from those delta frequencies. The calculated delta shear modulus, $\Delta\mu$, due to magnetic field is in the order of 10 MPa and the shear modulus for many thermoplastic polymers is on the order of 1 GPa. Therefore, the amount of shear modulus change induced by magnetic field is about 1% of the natural shear modulus without magnetic field. The 1% change is similar to what was reported by Ren et. al [43] using conventional measuring techniques. Figure 45 copied from [43] shows the change in elastic modulus with increasing magnetic field for a 15 x 15 x 45 mm bar of $Sm_{0.88}Dy_{0.12}Fe_{1.93}$ alloy particles suspended in Araldite LY5210/HY2954 epoxy. The figure shows the elastic modulus decreases with increases of applied magnetic field. It is important to point out that the measurement done in [43] was using an AC magnetic field and the elastic modulus was extracted from the change in resonance and anti-resonance frequencies of the measured strain in the composite bar. The paper by Ren et. al provides an analogy for the physical bases of the MQCM system. Similar to Ren et. al, the calculations presented in this appendix also extracts information on the changes to the mechanical properties from the changes in resonance frequency. The fact that results from the new MQCM instrument is in the same order of magnitude compared to results measure using other means by other people is encouraging and points to the validity of the new MQCM class of instrumentation. Further more, experiments such as the one performed in [43] can only measure the bulk mechanical properties while the MQCM instrument can measure thin films which can exhibit different properties than the bulk material.

Although the work of Ren et. al [43] showed a decrease in stiffness with magnetic field, the works of [15, 60] on magnetorheological elastomers also clearly demonstrated the increase of shear stiffness with applied magnetic field. However, again in their work, only bulk properties were measured due to limitation of available instrumentation. Currently no

instrument exist that can measure such mechanical property changes induced by magnetic field. The calculations and additional references presented here demonstrated that magnetic field induced stiffness change can shift the frequency of the QCM by the amounts measured in this thesis.

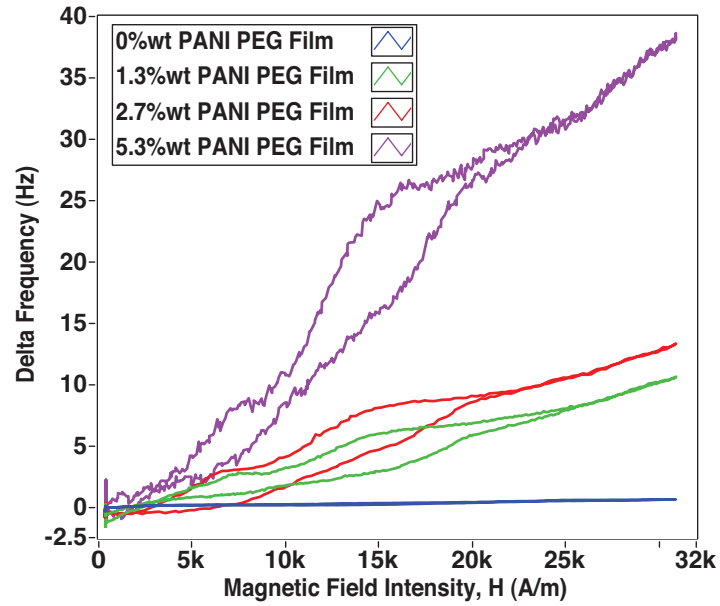**Figure 43:** MQCM raw delta frequency measured from undoped polyaniline suspended in poly(ethylene glycol).
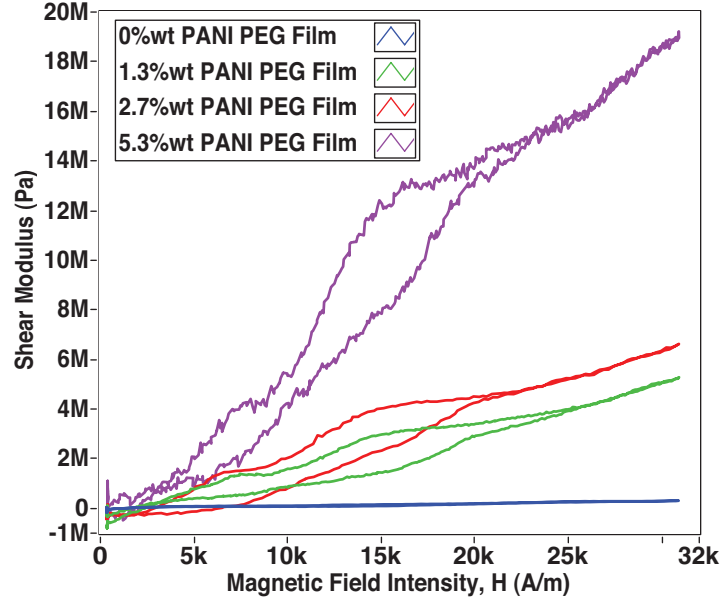
Figure 44: MQCM delta shear stiffness calculated from measured delta frequency for undoped polyaniline suspended in poly(ethylene glycol).
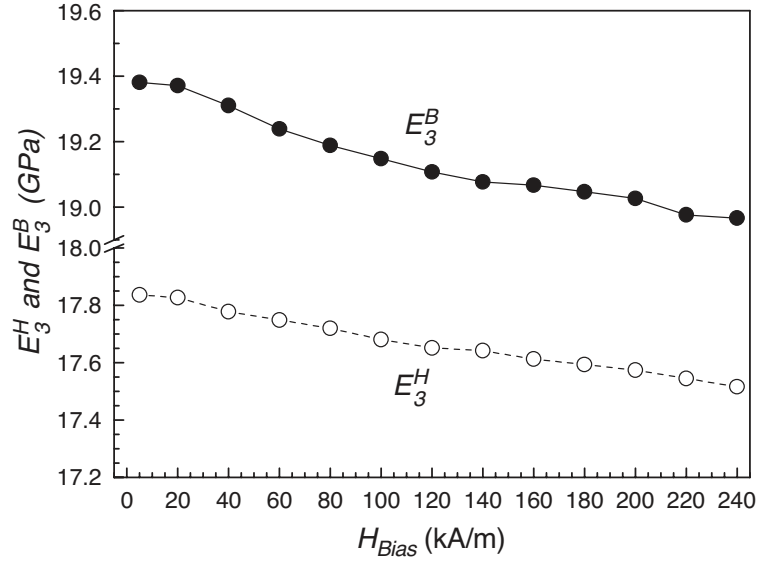

Figure 45: Dependence of elastic moduli at constant magnetic field strength E_3^H and at constant magnetic flux density E_3^B on magnetic bias field H_{Bias} [43].

61

REFERENCES

[1] ARNAU, A., *Piezoelectric Transducers and Applications.* Springer, 2004.

[2] ARNAU, A., SOGORB, T., and JIMENEZ, Y., "Circuit for continuous motional series resonant frequency and motional resistance monitoring of quartz crystal resonators by parallel capacitance compensation," *Review of Scientific Instruments*, vol. 73, no. 7, p. 2724, 2002.

[3] BRENDEL, R., CRETIN, B., and HABTI, A. E., "Origin and measurement of quartz resonator magnetic sensitivity," p. 260, 1994.

[4] BRENDEL, R., HASSANI, C. E., BRUNET, M., and ROBERT, E., "Influence of magnetic field on quartz crystal oscillators," p. 268, 1989.

[5] BRUCKENSTEIN, S. and SHAY, M., "An in-situ weighing study of the mechanism for the formation of the adsorbed oxygen monolayer at a gold electrode," *Journal of Electroanalytical Chemistry*, vol. 188, p. 131, 1985.

[6] BUTTRY, D. A. and WARD, M. D., "Measurement of interfacial processes at electrode surfaces with the electrochemical quartz crystal microbalance," *Chemical Reviews*, vol. 92, no. 6, p. 1355, 1992.

[7] CADY, W. G., "The piezo-electric resonator," *Proceedings of Institute of Radio Engineers*, vol. 10, p. 83, 1922.

[8] CASTRO, F. A. and GRAEFF, C. F. O., "Electrically detected and conventional magnetic resonance investigation of surface and bulk states in polyaniline thin films," *Journal of Applied Physics*, vol. 101, no. 083903, 2007.

[9] CHEN, Z. and LUO, R. C., "Design and implementation of capacitive proximity sensor using microelectromechanical systems technology," *IEEE Transactions on Industrial Electronics*, vol. 45, no. 6, p. 886, 1998.

[10] CLARK, J., "Squids," *Scientific American*, vol. 271, no. 2, p. 36, 1994.

[11] DAIKHIN, L., GILEADI, E., KATZ, G., TSIONSKY, V., URBAKH, M., and ZAGIDULIN, D., "Influence of roughness on the admittance of the quartz crystal microbalance immersed in liquids," *Analytical Chemistry*, vol. 74, pp. 554–561, 2002.

[12] DUNHAM, G. C., BENSON, N. H., PETELENZ, D., and JANATA, J., "Dual quartz crystal microbalance," *Analytical Chemistry*, vol. 67, pp. 267–272, 1995.

[13] FITE, C., CAO, Y., and HEEGER, A. J., "Magnetic susceptibility of crystalline polyaniline," *Solid State Communications*, vol. 70, no. 3, p. 245, 1989.

[14] FONER, S., "Review of magnetometry," *IEEE Transactions on Magnetics*, vol. MAG-17, no. 6, p. 3358, 1981.

[15] GONG, X. L., ZHANG, X. Z., and ZHANG, P. Q., "Fabrication and characterization of isotropic magnetorheological elastomers," *Polymer Testing*, vol. 24, no. 5, p. 669, 2005.

[16] GRATE, J. W., "Acoustic wave microsensor arrays for vapor sensing," *Chemical Reviews*, vol. 100, no. 7, p. 2627, 2000.

[17] GRATE, J. W., MARTIN, S. J., and WHITE, R. M., "Acoustic wave microsensors," *Analytical Chemistry*, vol. 65, p. 940, 1993.

[18] GREBENIKOV, V. N., MANORIK, P. A., SHULZHENKO, A. V., and FEDORENKO, M. A., "Piezoquartz microbalance in nonuniform magnetic field the new method for research of magnetic properties," *Journal of Physical Chemistry (Rus)*, vol. 77, no. 6, p. 1113, 2003.

[19] HUNT, W. D., STUBBS, D. D., and LEE, S. H., "Time-dependent signatures of acoustic wave biosensors," *Proceedings of The IEEE*, vol. 91, no. 6, p. 890, 2003.

[20] INOUE, M., TSUBOI, Y., YOKOKAWA, N., and FUJII, T., "Love-type magneto-surface-acoustic-wave in multilayered highly magnetostrictive films separated by insulating layers," *IEEE Transactions on Magnetics*, vol. 26, no. 5, p. 1465, 1990.

[21] JAGIELLA, M., FERICEAN, S., and DORNEICH, A., "Progress and recent realizations of miniaturized inductive proximity sensors for automation," *IEEE Sensors Journal*, vol. 6, no. 6, p. 1734, 2006.

[22] JANATA, J. and JOSOWICZ, M., "Chemical modulation of work function as a transduction mechanism for chemical sensors," *Accounts of Chemical Research*, vol. 31, p. 241, 1998.

[23] JANATA, J. and JOSOWICZ, M., "Conducting polymers in electronic chemical sensors," *Nature Materials*, vol. 2, p. 19, 2003.

[24] JANSHOFF, A., GALLA, H., and STEINEM, C., "Piezoelectric mass-sensing devices as biosensors - an alternative to optical biosensors?," *Angewandte Chemie International Edition*, vol. 39, no. 22, p. 4004, 2000.

[25] JEONG, C. K., JUNG, J. H., KIM, B. H., LEE, S. Y., LEE, D. E., JANG, S. H., RYU, K. S., and JOO, J., "Electrical, magnetic, and structural properties of lithium salt doped polyaniline," *Synthetic Metals*, vol. 117, no. 1-3, p. 99, 2001.

[26] JOHANNSMANN, D., "Derivation of the shear compliance of thin ?lms on quartz resonators from comparison of the frequency shifts on different harmonics: A perturbation analysis," *Journal of Applied Physics*, vol. 89, no. 11, p. 6356, 2001.

[27] JOSSE, F., SHANA, Z. A., and ZONG, H., "Propagation of acoustic waves at the interface between a piezoelectric crystal and an isotropic viscoelastic conductive medium," *Proceedings IEEE Ultrasonic Symposium*, vol. 1, pp. 289–94, 1992.

[28] JR., W. H. K., "Piezoelectric sorption detector," *Analytical Chemistry*, vol. 36, no. 9, p. 1735, 1964.

[29] KAHOL, P. K., RAGHUNATHAN, A., and McCORMICK, B. J., "A magnetic suscepti-bility study of emeraldine base polyaniline," *Synethetic Metals*, vol. 140, no. 2-3, p. 261, 2004.

[30] LONG, Y., CHEN, Z., SHEN, J., ZHANG, Z., ZHANG, L., XIAO, H., WANG, M., and DUVAIL, J. L., "Magnetic properties of conducting polymer nanostructures," *Journal of Physical Chemistry B*, vol. 110, no. 46, p. 23228, 2006.

[31] LU, C., "Investigation of film-thickness determination by oscillating quartz resonators with large mass load," *Journal of Applied Physics*, vol. 43, no. 11, p. 4385, 1972.

[32] LU, C., *Applications of Piezoelectric Quartz Crystal Microbalances*. Elsevier, 1984.

[33] MARTIN, S. J. and FRYE, G. C., "Polymer film characterization using quartz res-onators," *Proceedings of IEEE Ultrasonics Symposium*, vol. 1, p. 393, 1998.

[34] MAXWELL, J. C., "On physical lines of force," *London, Edinburgh, and Dublin Philo-sophical Magazine and Journal of Science*, 1861.

[35] McKNIGHT, G. P. and CARMAN, G. P., "Energy absorption in axial and shear loading of particulate magnetostrictive composites," *Proceedings of SPIE*, vol. 3992, p. 572, 2000.

[36] MILEWSKI, A., SAMULA, J., MAKSYMOWICZ, L. J., WENDA, J., JANKOWSKI, H., and KULAK, A., "Multilayer structure of metallic glass films in a variable saw delay line," *Thin Solid Films*, vol. 175, p. 335, 1989.

[37] MISRA, S. C. K., PANT, R. P., PANDEY, J. L., and KUMAR, N., "Preparation and characterization of magnetic polymeric," *Journal of Magnetism and Magnetic Materi-als*, vol. 252, p. 20, 2002.

[38] ORCHARD, A. F., *Magnetochemistry*. Oxford University Press, 2003.

[39] PETR, A., NEUDECK, A., and DUNSCH, L., "On the magnetic susceptibility of polyani-line an alternative approach," *Chemical Physics Letters*, vol. 401, p. 130, 2005.

[40] POTJE-KAMLOTH, K., POLK, B. J., JOSOWICZ, M., and JANATA, J., "Photochemical tuning of field-effect transistor with polyaniline gate conductor," *Advanced Materials*, vol. 13, no. 23, p. 1797, 2001.

[41] POTJE-KAMLOTH, K., POLK, B. J., JOSOWICZ, M., and JANATA, J., "Doping of polyaniline in the solid state with photogenerated triflic acid," *Chemistry of Materials*, vol. 14, no. 6, p. 2782, 2002.

[42] REED, C. E., KANAZAWA, K. K., and KAUFMAN, J. H., "Physical description of a viscoeleastically loaded at-cut quartz resonator," *Journal of Applied Physics*, vol. 68, no. 5, p. 1993, 1989.

[43] REN, W. J., OR, S. W., CHAN, H. L. W., and ZHANG, Z. D., "Magnetoelastic properties of polymer-bonded $sm_{0.88}dy_{0.12}fe_{1.93}$," *Journal of Magnetism and Magnetic Materials*, vol. 293, no. 3, p. 908, 2005.

[44] RODAHL, M., HÖÖK, F., and KASEMO, B., "Qcm operation in liquids: An explanation of measured variations in frequency and q factor with liquid conductivity," *Analytical Chemistry*, vol. 68, no. 13, p. 2219, 1996.

[45] RODAHL, M. and KASEMO, B., "A simple setup to simultaneously measure the resonant frequency and the absolute dissipation factor of a quartz crystal microbalance," *Review of Scientific Instruments*, vol. 67, no. 9, p. 3238, 1996.

[46] SAUERBREY, G. *Zeitschrift fr Physik*, vol. 155, no. 155, p. 206, 1959.

[47] SHANA, Z. A. and JOSSE, F., "Analysis of electrical equivalent circuit of quartz crystal resonator loaded with viscous conductive liquids," *Analytical Chemistry*, vol. 66, pp. 1955–1964, 1994.

[48] SITTEL, K., JR., P. E. R., and BAILEY, E. D., "Method for determining the viscoelastic properties of dilute polymer solutions at audio-frequencies," *Journal of Applied Physics*, vol. 25, no. 10, p. 1312, 1954.

[49] SMITH, J. A., JOSOWICZ, M., and JANATA, J., "Gold-polyaniline composite," *Physical Chemistry Chemical Physics*, vol. 7, p. 3614, 2005.

[50] STEINEM, A. J. C. and JANSHOFF, A., *Piezoelectric Sensors*. Springer, 2006.

[51] SYED, A. and DINESAN, M., "Review: Polyaniline - a novel polymeric material," *Talanta*, vol. 38, no. 8, p. 815, 1991.

[52] THOMPSON, M., BALLANTYNE, S. M., CHERAN, L. E., STEVENSON, A. C., and LOWE, C. R., "Electromagnetic excitation of high frequency acoustic waves and detection in the liquid phase," *The Analyst*, vol. 128, p. 1048, 2003.

[53] WEBB, D. C., FORESTER, D. W., GANGULY, A. K., and VITTORIA, C., "Applications of amorphous magnetic-layers in surface-acoustic-wave devices," *IEEE Transactions on Magnetics*, vol. 15, no. 6, p. 1410, 1979.

[54] WIEGERT, R. F. and LEVY, M., "Magnetic field dependence of surface acoustic wave velocity and attenuation in nickel thin films," *Journal of Applied Physics*, vol. 64, no. 10, p. 5411, 1988.

[55] YAMAGUCHI, M., HASHIMOTO, K. Y., KOGO, H., and NAOE, M., "Variable saw delay line using amorphous tbfe2 film," *IEEE Transactions on Magnetics*, vol. 16, no. 5, p. 916, 1980.

[56] YANG, M. and THOMPSON, M., "Acoustic network analysis and equivalent circuit simulation of the thickness-shear mode acoustic wave sensor in the liquid phase," *Analytica Chimica Acta*, vol. 282, p. 505, 1993.

[57] YANG, M. and THOMPSON, M., "Perturbation of the electrified interface and the response of the thickness-shear mode acoustic wave sensor under conductive liquid loading," *Analytical Chemistry*, vol. 65, pp. 3591–3597, 1993.

[58] YU, G. Y. and JANATA, J., "Proximity effect in quartz crystal microbalance," *Analytical Chemistry*, vol. 80, no. 8, p. 2751, 2008.

[59] YU, G. Y., JOSOWICZ, M., HUNT, W. D., and JANATA, J., "Development of a magnetic quartz crystal microbalance," *Review of Scientific Instruments*, vol. 78, no. 6, p. 065111, 2007.

[60] ZHOU, G. Y., "Shear properties of a magnetorheological elastomer," *Smart Materials and Structures*, vol. 12, no. 1, p. 139, 2003.

[61] ZHOU, M., MYUNG, N., CHEN, X., and RAJESHWAR, K., "Electrochemical deposition and stripping of copper, nickel and copper nickel alloy thin films at a polycrystalline gold surface: a combined voltammetry-coulometry-electrochemical quartz crystal microgravimetry study," *Journal of Electroanalytical Chemistry*, vol. 398, no. 1, p. 5, 1995.

VITA

George Y. Yu received his B.S. Degree in Electrical Engineering from Georgia Institute of Technology in 2004 and his M.S. Degree in Electrical and Computer Engineering from the Georgia Institute of Technology in 2006. He is expected to receive his Ph.D. Degree in Electrical and Computer Engineering from the Georgia Institute of Technology in 2008. His graduate research focused on the developing a radical new magnetic instrument using combined inter-related disciplines of Electrical Engineering, Chemistry, and Physics.

Publications:

Yu, G. Y., Josowicz, M., Hunt, W. D., and Janata, J., "Development of a magnetic quartz crystal microbalance," *Review of Scientific Instruments*, vol. 78, no. 6, p. 065111, 2007.

Yu, G. Y. and Janata, J., "Proximity effect in quartz crystal microbalance," *Analytical Chemistry*, vol. 80, no. 8, p. 2751, 2008.

Yu, G. Y. and Janata, J., "Magnetic Quartz Crystal Microbalance: A Multi-layer Gold/Nickel Stack," *Journal of Applied Physics*, Submitted April 2008.